NOTICE

The quality of this microfiche is heavily dependent upon the quality of the original thesis submitted for microfilming. Every effort has been made to ensure the highest quality of reproduction possible.

If pages are missing, contact the university which granted the degree.

Some pages may have indistinct print especially if the original pages were typed with a poor typewriter ribbon or if the university sent us a poor photocopy.

Previously copyrighted materials (journal articles, published tests, etc.) are not filmed.

Reproduction in full or in part of this film is governed by the Canadian Copyright Act, R.S.C. 1970, c. C-30. Please read the authorization forms which accompany this thesis.

THIS DISSERTATION
HAS BEEN MICROFILMED
EXACTLY AS RECEIVED

AVIS

La qualité de cette microfiche dépend grandement de la qualité de la thèse soumise au microfilmage. Nous avons tout fait pour assurer une qualité supérieure de reproduction.

S'il manque des pages, veuillez communiquer avec l'université qui a conféré le grade.

La qualité d'impression de certaines pages peut laisser à désirer, surtout si les pages originales ont été dactylographiées à l'aide d'un ruban usé ou si l'université nous a fait parvenir une photocopie de mauvaise qualité.

Les documents qui font déjà l'objet d'un droit d'auteur (articles de revue, examens publiés, etc.) ne sont pas microfilmés.

La reproduction, même partielle, de ce microfilm est soumise à la Loi canadienne sur le droit d'auteur, SRC 1970, c. C-30. Veuillez prendre connaissance des formules d'autorisation qui accompagnent cette thèse.

LA THÈSE A ÉTÉ
MICROFILMÉE TELLE QUE
NOUS L'AVONS REÇUE

STUDY OF MICROSTRIP TRIANGULAR RESONATORS

by

Misel Cuhaci

A thesis submitted to the School of Graduate Studies,
University of Ottawa, in partial fulfilment
of the requirements for the degree of
Master of Applied Science.

Department of Electrical Engineering
Faculty of Science and Engineering
University of Ottawa
Ottawa, Ontario
April, 1979.

ACKNOWLEDGEMENTS

The author would very much like to acknowledge the guidance and encouragement of his superviser Dr. W.J.R. Hoefer. The author is also grateful to Dr. D.S. James for his suggestions and encouragement, to Dr. L. Shafai for his helpful discussions and to his colleagues and friends at the Space Electronics Directorate of the Communications Research Centre where this work was conducted.

Finally the financial assistance received from the Department of Electrical Engineering, University of Ottawa, during the course of this thesis is also gratefully appreciated.

ABSTRACT

The radiation properties of microstrip triangular resonators are investigated. Both the radiation pattern and the radiation quality factor (Q_r) are derived analytically utilizing the current distribution on the resonator and numerical techniques. The different loss mechanisms of the microstrip resonators are described. The radiation losses were determined experimentally. Computed and experimental results are in reasonable agreement. The equivalent lumped circuit parameters of the resonator as well as some possible applications are also discussed.

LIST OF CONTENTS

LIST OF TABLES

LIST OF FIGURES

LIST OF FIGURES - Contd

CHAPTER I

INTRODUCTION

1.1 INTRODUCTION

Stripline or microstrip structures are being used more and more at microwave and millimeter wave frequencies. The structure consists of a conductive strip deposited on a dielectric substrate backed by a conductive ground plane Fig. 1.1. The electromagnetic properties depend on the geometry, such as strip width w, strip thickness t, and substrate thickness h, the dielectric and magnetic properties of the substrate and the medium (usually air) above it.

This planar configuration is small and consequently lighter; circuits fabricated with this technique are cheaper than waveguide or coaxial systems. Also, beam-leaded active or passive devices can be bonded directly to the conductor strip on the dielectric substrate [1]. Ultimately, the planar configuration lends itself to the fabrication of integrated circuits.

However, the applications of Microwave Integrated Circuits (MIC) as transmission medium at microwave frequencies are limited by a number of factors such as line attenuation due to dielectric and resistive losses, breakdown effects at high power levels and radiation from discontinuities. The last effect which constrains the microwave circuit

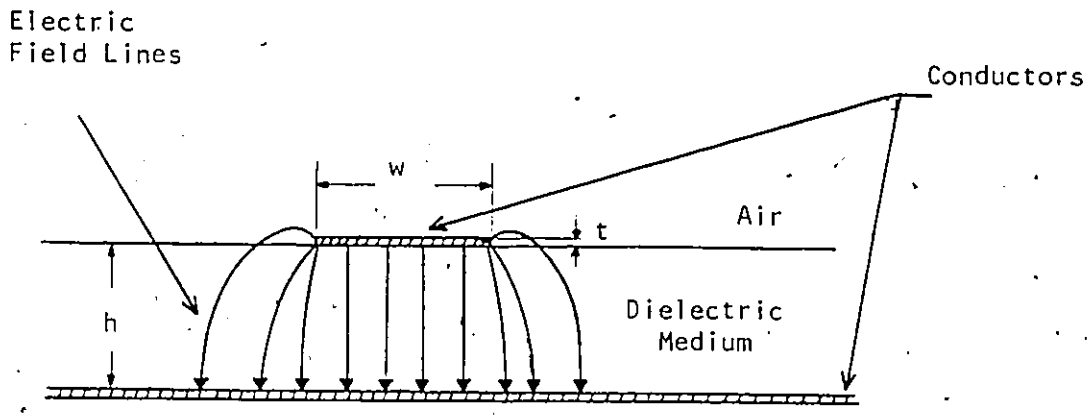

Fig. 1.1 - Microstrip Structure

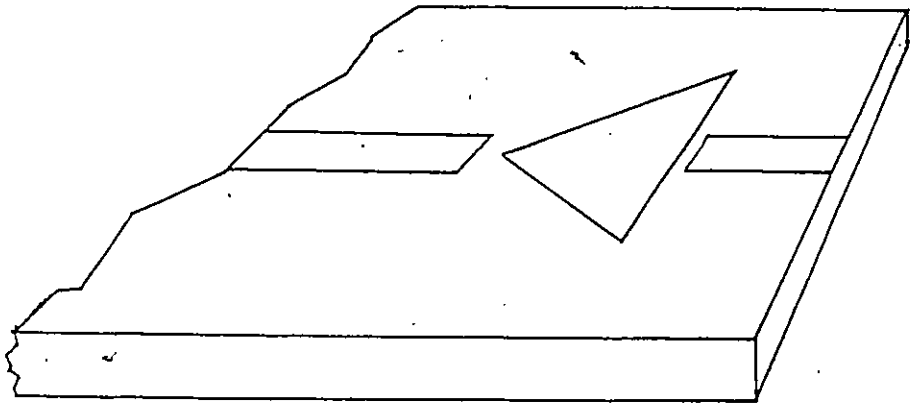

Fig. 1.2 - Triangular Microstrip Resonator

designer but represents a desired property for an antenna engineer, constitutes one of the major problems in MIC circuit design. The analysis of the power radiated from these structures is complicated by the fact that two different dielectric media (air and substrate) are present simultaneously.

Resonators are one of the basic building blocks for the microwave engineer, as they are used to design filters, circulators, oscillators etc. A resonant element in MIC generally presents a discontinuity to the transmitted signal. The poor quality factor of the microstrip resonators, which is due to dielectric and resistive losses, is further aggravated by the power radiated from the discontinuities.

There are numerous papers analysing the performance of different resonators, e.g. the rectangular, disc, ring, etc. The equilateral triangle and the disc resonators are of special interest because of the 120^{o} symmetry. For the triangular resonator Fig. 1.2, some studies have been carried out by Hoefer, Helszajn and James [2,3] to determine the electric and magnetic fields and to calculate the resonant frequencies of the different modes.

In this thesis, the triangular microstrip resonator will be analysed. The theoretical expression for the radiation will be derived and compared with experimental results.

1.2 LITERATURE SURVEY OF THE THEORETICAL AND EXPERIMENTAL STUDIES ON THE LOSSES IN MICROSTRIP RESONATORS.

In February 1960, Lewin [4] published a paper describing the "Radiation From Discontinuities In Strip-line". In this article a method to derive the theoretical radiation expressions from the known current distribution is presented. A rigorous analysis of the radiation from microstrip was found to be difficult because of the complex transmission medium and therefore the author of the paper made some simplifying assumptions. The method so developed was used to study transmission line configurations like the open-circuit, matched co-axial termination, mismatched termination, parallel post resonator formed by two parallel posts and the right-angle corner. His results were approximate but it was shown later by other authors [2,5,6,9] that there was reasonable agreement with measurements.

In April 1969, Denlinger [5] gave some experimental results showing the relation between microstrip parameters and the fractional amount of power radiated from a resonant line. He verified that the percentage of the power radiated depends on the thickness of the substrate. The measurements agreed with the values Lewin calculated for the case of an open-circuit microstrip line. He also made radiation measurements on the disc resonator and derived some empirical conclusions.

In October 1969, Watkins [6] analysed the mode patterns of circular disc resonators. Referring to Troughton's [7] work on high Q-factor resonators, he expected low radiation losses for the dominant mode in the circular structure. A short report by the same author [8] on the

radiation loss from open-circuit resonators appeared in October 1973. In this article he discussed the conductor, dielectric and radiation losses of a rectangular resonator and showed that an extension to Lewin's analysis could yield the radiation loss of this geometry. He also suggested using the structure as an antenna element after considering the radiation patterns of different modes.

In September 1970, Easter and Roberts [9] described the calculations of the radiation loss of a half-wavelength open-circuit resonator and gave results for a range of different effective permittivities. They used Lewin's method [4] to derive the theoretical expressions which were then checked experimentally. The same authors published another paper [10] in April 1971 where they compared different types of resonators, namely the ring, open-circuit linear, short-circuit linear and the "hairpin" or "U" shaped resonator. They showed that the hairpin resonator radiates less than the straight resonator.

Sobol's study of the radiation conductance of open-circuit microstrip [11] appeared in November 1971. He calculated the radiation conductance at the open-circuit end of a microstrip stub and used the result to find the total loss of that configuration. He found good agreement between his results and Denlinger's results [5].

In June 1975, Belohoubek and Denlinger [12] studied the loss mechanism of microstrip resonators. They derived formulae for the radiation Q of open-circuit microstrip resonators based on Lewin's work [4]. They described the effect of radiation on the overall circuit Q as a function of the characteristic impedance, frequency, dielectric constant

and substrate thickness. These results showed that radiation losses at higher frequencies dominate over the conductor and dielectric losses; they also showed that microstrip lines on substrates with a low dielectric constant radiate more.

There are also papers published on microstrip antennas using the rectangular or circular resonators as basic elements. Howell [13] discussed these two configurations in his paper which appeared in January 1975. He gave design procedures for linearly and circularly polarized antennas and also presented the measured radiation patterns.

The work of Morel et al. [15] on the theoretical investigation of the circular disc antenna appeared in April 1976. The far-field total radiated power and power losses were calculated. These expressions were derived considering air as the dielectric separating the conducting plates. Also, approximate results were derived for the various dielectric materials. At the same time Walton et al [16] investigated experimentally the radiation characteristics of circular discs. They studied the antenna elements with regard to their driving point impedances and far-field radiation patterns.

In November 1976, Derneryd [14] studied linearly polarized microstrip antennas. He characterized the square and rectangular elements by their radiation pattern, directivity and equivalent admittance. Also, he gave a design procedure for open-circuit halfwave resonators and for arrays of resonators.

1.3 THESIS SUMMARY

The object of this thesis is to study theoretically and experimentally the radiation loss of an equilateral triangular microstrip resonator. An approach similar to Lewin's [4] was taken to derive the theoretical expressions for the radiation pattern and the radiation quality factor, Q_r. Numerical methods were used to obtain the theoretical results which were then compared to the measurements. The measured radiation Q-factor of the triangular structure was also compared with that of a circular resonator.

The resonators were studied experimentally as lossy microstrip circuit elements and their unloaded Q-factor, Q_o, was measured in each sample for both the open and shielded case. Neglecting the losses due to imperfect shielding, the discrepancy in the two measurements was attributed to the radiation loss.

Different coupling configurations to the microstrip resonators were described and the equivalent circuit for the resonator was studied.

To conclude, the use of a triangular resonator as a circuit and antenna element were briefly discussed.

CHAPTER II

FIELD AND CURRENT DISTRIBUTION IN THE TRIANGULAR RESONATOR

2.1 INTRODUCTION

Microstrip structures are studied, in general, by replacing the planar configuration with an equivalent waveguide model which consists of electric walls to replace the conductors, and of magnetic walls on the sides to contain the electric field. Solutions for the fields and cut-off frequencies for a waveguide with an equilateral triangular cross-section are described by Schelkunoff [20]. These results were applied to predict the resonances of triangularly shaped microstrip resonators by Hoefer, Helszajn and James [2,3]. Their work, as summarized in the first section below, provides a basis for the radiation analysis. To simplify the analysis, the Hertz vector will also be introduced in this Chapter.

2.2 ELECTRICAL AND MAGNETIC PROPERTIES OF THE TRIANGULAR RESONATOR

The $TM_{m,n,\ell}$* mode field patterns in the triangular resonator filled with a dielectric material of permittivity ϵ, permeability μ and with no variation of the field along the thickness of the structure are given by:

---

* The TM-modes are defined such that the magnetic field possesses components in the xy-plane only, since the field equations have been derived originally in a waveguide of triangular cross-section.

$$E_z = A_{m,n,\ell} \; T(x,y)_{m,n,\ell} \qquad \ldots\ldots (2.1)$$

$$H_x = \frac{j}{\omega\mu} \frac{\delta E_z}{\delta y} \qquad \ldots\ldots (2.2)$$

$$H_y = \frac{-j}{\omega\mu} \frac{\delta E_z}{\delta x} \qquad \ldots\ldots (2.3)$$

$$H_z = E_x = E_y = 0 \qquad \ldots\ldots (2.4)$$

where

i) $A_{m,n,\ell}$ is an arbitrary amplitude factor

ii) $$T(x,y)_{m,n,\ell} = \cos\left[\left(\frac{2\pi x}{\sqrt{3}a} + \frac{2\pi}{3}\right)\ell\right] \cos\left[\frac{2\pi(m-n)y}{3a}\right] + \cos\left[\left(\frac{2\pi x}{\sqrt{3}a} + \frac{2\pi}{3}\right)m\right] \cos\left[\frac{2\pi(n-\ell)y}{3a}\right] + \cos\left[\left(\frac{2\pi x}{\sqrt{3}a} + \frac{2\pi}{3}\right)n\right] \cos\left[\frac{2\pi(\ell-m)y}{3a}\right] \qquad (2.5)$$

where "a" is the side of the triangle

iii) m, n, ℓ are integers which are never zero simultaneously and satisfy the condition

$$m + n + \ell = 0 \qquad (2.6)$$

The resonant frequencies are:

$$f_{o_{m,n,\ell}} = \frac{1}{2} (\varepsilon\mu)^{-\frac{1}{2}} \left[\left(\frac{4}{3a} \right)^2 (m^2+mn+n^2) \right]^{\frac{1}{2}} \quad \ldots.(2.7)$$

with $\varepsilon = \varepsilon_o \varepsilon_r$ and $\mu = \mu_o \mu_r$

where ε_r and μ_r are the relative dielectric constant and the relative permeability.

Fig. 2.1 shows the $TM_{0,1,-1}$ mode which is associated with the lowest resonant frequency in a triangular resonator.

The energy stored in the structure is expressed by:

$$W_{\substack{stored \\ m,n,\ell}} = \frac{\varepsilon h}{2} A^2_{m,n,\ell} \int_S \left[T(x,y)_{m,n,\ell} \right]^2 dS \quad \ldots.(2.8)$$

where he is the microstrip thickness and S is the surface area of the triangle.

The above expressions are general. For the particular case analysed here, m = 1, n = 0 and ℓ = -1. This is the case of the dominant $TM_{1,0,-1}$ mode for which the expressions (2.1) to (2.8) can be written as:

$$E_z(x,y,z) = A_{1,0,-1} \left[2 \cos \left(\frac{2\pi x}{\sqrt{3}a} + \frac{2\pi}{3} \right) \cos \frac{2\pi y}{3a} + \cos \frac{4\pi y}{3a} \right] \quad \ldots.(2.9)$$

$$H_x(x,y,z) = -j A_{1,0,-1} \xi_o \left[\cos \left(\frac{2\pi x}{\sqrt{3}a} + \frac{2\pi}{3} \right) \cos \frac{2\pi}{3a} y + \sin \frac{4\pi}{3a} y \right] \quad ..(2.10)$$

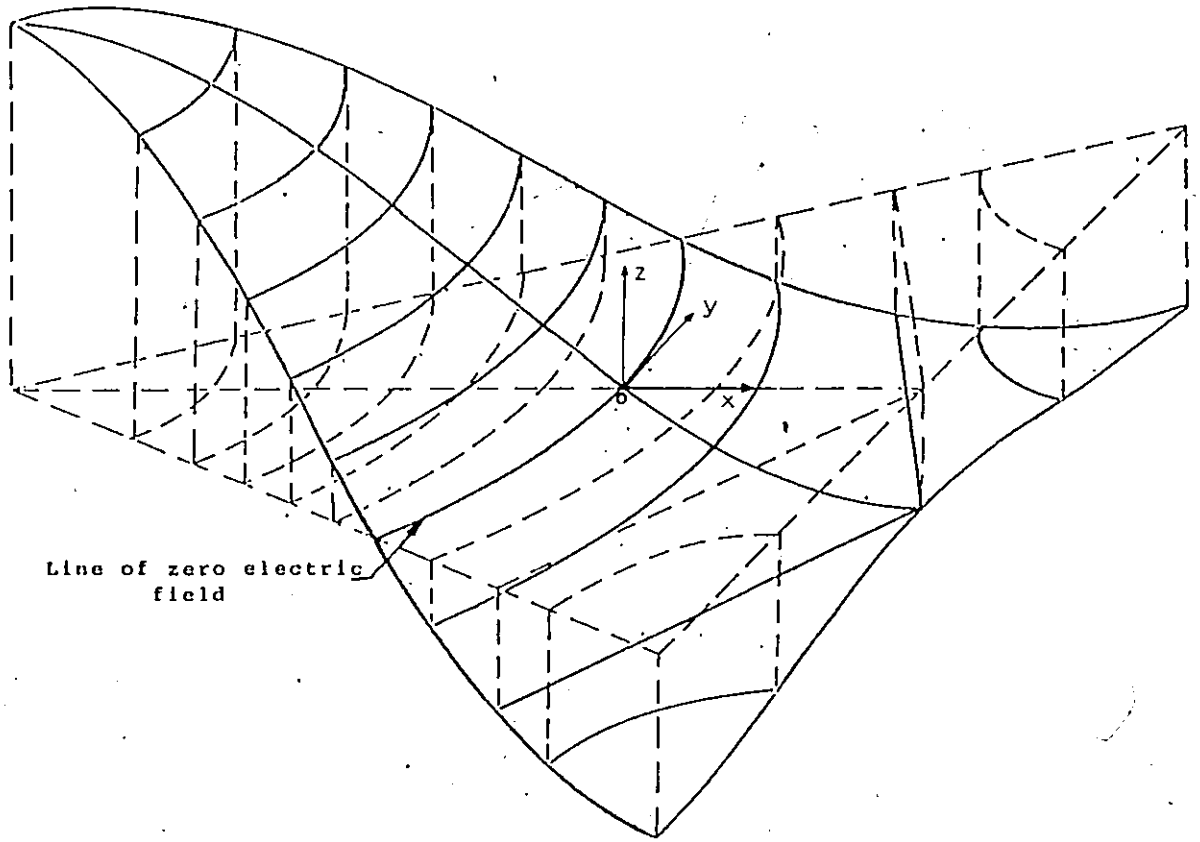

Fig. 2.1 - Magnitude of the electric field of the fundamental resonant mode ($TM_{0,1,-1}$) in a triangular resonator. The dotted lines in the triangular plane indicate magnetic field lines. (from ref.2)

$$H_y(x,y,z) = j\sqrt{3}\ A_{1,0,-1}\ \xi_o \left[\sin\left(\frac{2\pi x}{\sqrt{3}a} + \frac{2\pi}{3}\right)\ \cos\ \frac{2\pi}{3a}y\right] \quad \ldots(2.11)$$

with $\xi_o = \sqrt{\frac{\varepsilon_o}{\mu_o}} = \frac{1}{120\pi}\ S$ $\quad \ldots(2.12)$

The fundamental frequency of resonance is:

$$f_{o_{1,0,-1}} = \frac{2c}{3a\sqrt{\varepsilon_r}} \quad \ldots(2.13)$$

where $c = 3 \times 10^8$ m/s

The stored energy, after carrying out the integration becomes:

$$W_{\substack{\text{stored} \\ 1,0,-1}} = \frac{3\sqrt{3}}{16}\ \varepsilon h a^2 A^2_{1,0,-1} \quad \ldots(2.14)$$

2.3 ELECTROMAGNETIC FIELDS IN TERMS OF THE HERTZ VECTOR

The Hertz vector, $\vec{\Pi}$, is a mathematical quantity, which can be used to express other field quantities by means of simple operators. The derivation for the following equation can be found in the literature [21].

$$\vec{\Pi} = \frac{-j}{4\pi}\sqrt{\frac{\mu_o}{\varepsilon_o}}\ \frac{1}{k\varepsilon_r} \int_\tau \frac{\exp(-jk\sqrt{\mu_r\varepsilon_r}\ r)}{r}\ \vec{J}\ d\tau \quad \ldots(2.15)$$

where $\vec{J}$ is the vector representing the current distribution on the radiating element, in A/m^2.

τ is the volume surrounding the source, in m^3.

r is the radial distance in meter from the source to a point in space

ϵ_r and μ_r are respectively the relative permittivity and permeability of the space

$k = \frac{2\pi}{\lambda}$ in m^{-1} (wave number)

λ is the wavelength in the free space.

In terms of the Hertz vector, the electric and magnetic fields, at any point in the space containing the source, can be written as

$$\vec{E} = \nabla(\nabla \cdot \vec{\Pi}) + k^2 \epsilon_r \mu_r \vec{\Pi} \qquad \ldots(2.16)$$

$$\vec{H} = j\, k \sqrt{\frac{\epsilon_o}{\mu_o}}\, \epsilon_r\, (\nabla \times \vec{\Pi}) \qquad \ldots(2.17)$$

It can be seen from the above expressions that the knowledge of the complete or entire current distribution in a structure, with a defined geometry, is sufficient to derive the electric and magnetic fields radiating into space.

2.4 THE CURRENT DISTRIBUTION IN THE TRIANGULAR RESONATOR

The current in a microstrip structure is the vectorial sum of two currents, namely the conduction and the dielectric polarization current.

a) The conduction current density;

In perfect conductors, the current flow at high frequencies can be considered as a true surface current due to the "skin effect". Inside the conductor there is no displacement current, and a time varying magnetic field does not exist. On the surface, the conduction current density is,

$$\vec{J}_c = \vec{n} \times \vec{H} \qquad \ldots.(2.18)$$

where $\vec{n}$ is the unit vector orthogonal to $\vec{H}$, the magnetic field.

To ensure low resistive losses, for all practical microstrip configurations, the conductors are a few skin depths thick. This implies that the displacement current is entirely under the metallization and the conductors can be replaced by a current sheet for analytical purposes. Also the ground plane can be replaced by the image of the top conductor Fig. 2.2. The latter is a valid transformation since generally the ground plane is much larger in surface area than the triangular conductor.

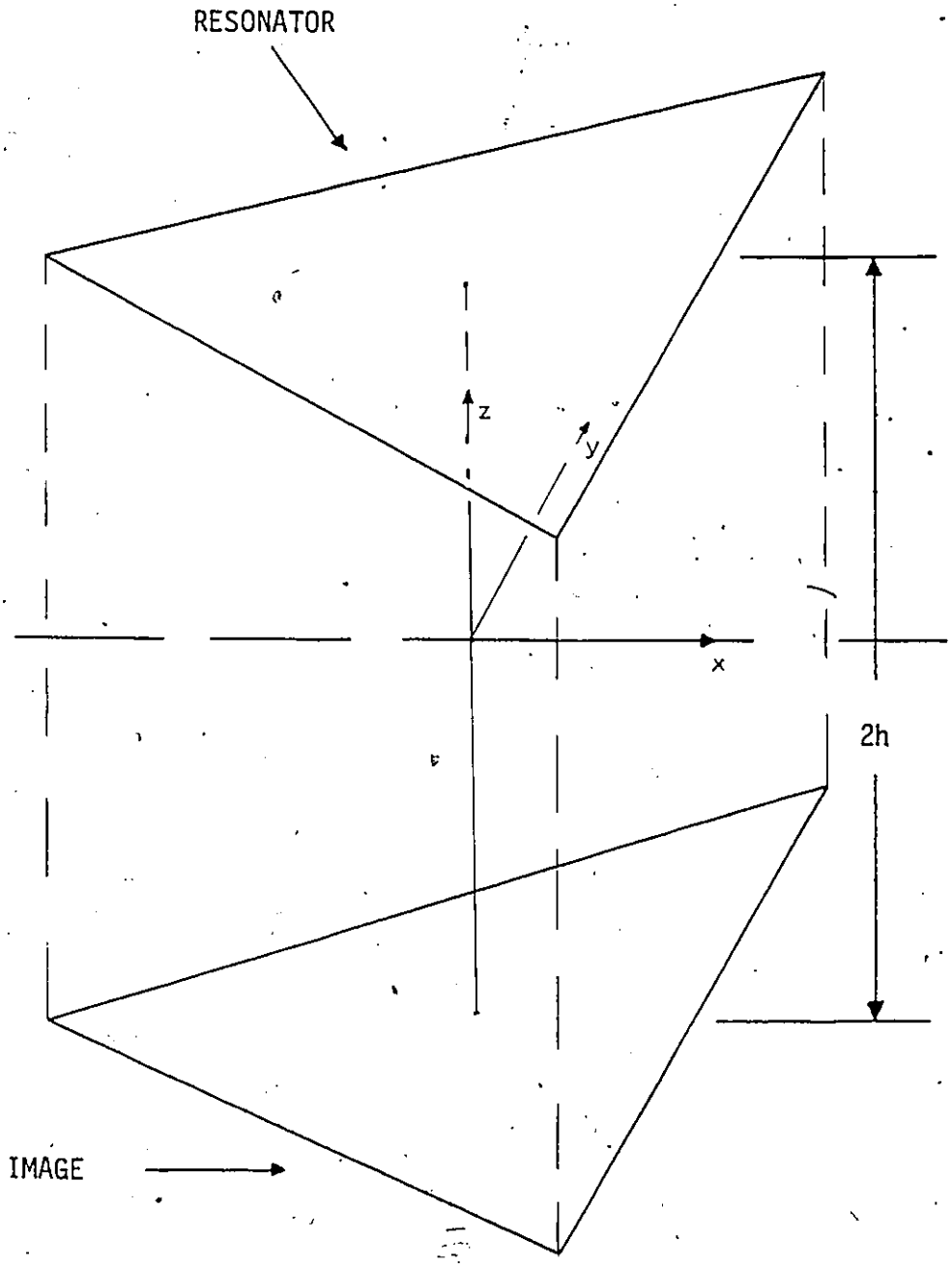

Fig. 2.2 - Resonator and Image Configuration

The expression for the magnetic field vector, assuming $\vec{H}$ is constant along the z-axis is:

$$\left.\begin{aligned} \vec{H} &= H_x\,(x,y,h)\vec{a}_x + H_y\,(x,y,h)\vec{a}_y \\ \text{and} \quad \vec{n} &= \vec{a}_z \end{aligned}\right\} \qquad \ldots(2.19)$$

where $\vec{a}_x$, $\vec{a}_y$, $\vec{a}_z$ are unit direction vectors.

The error introduced by the above approximation is negligible as long as the thickness h, of the substrate is much smaller than the guided wavelength λ_g. The conduction current density $\vec{J}_{cr}$, on the resonator, at z = h, is obtained from (2.18).

$$\vec{J}_{cr} = -H_y\,(x,y,h)\,\vec{a}_x + H_x\,(x,y,h)\,\vec{a}_y \qquad \ldots(2.20)$$

The image of the current density $\vec{J}_{cr}$, at z = -h, is,

$$\vec{J}_{ci} = H_y\,(x,y,-h)\,\vec{a}_x - H_x\,(x,y,-h)\,\vec{a}_y \qquad \ldots(2.21)$$

b) The dielectric polarization current density;

Maxwell's equation can be modified to emphasize the contribution of the polarization current to the total current (4).

$$\nabla \times \vec{H} = j\frac{k}{120\pi}\vec{E} + (\vec{J} + j\frac{k}{120\pi}(\epsilon - 1)\vec{E}) \quad \ldots(2.22)$$

where $$\frac{1}{120\pi} = \sqrt{\frac{\epsilon_o}{\mu_o}}$$

The above expression shows that the dielectric polarization acts as an impressed current density, $\vec{J}_p$:

$$\vec{J}_p = j\frac{k}{120\pi}(\epsilon - 1)\vec{E} \quad \ldots(2.23)$$

In a microstrip structure, ϵ is a function of z, for $z > h$, $\epsilon = \epsilon_{air}$, and for $z \leq h$, $\epsilon = \epsilon_r$ of the dielectric. The analysis will be simplified by taking ϵ as the effective permittivity, ϵ_e^*, of the substrate material. Due to this approximation, as $\epsilon_{air} < \epsilon_e < \epsilon_r$, the contribution of the polarization current is under-valued in between the conductors and over-valued above. The polarization current density is independent of z, and for simplicity, it is taken at $z = 0$.

$$\vec{J}_p(x,y,z) = \vec{J}_p(x,y,o) = j\frac{k}{120\pi}(\epsilon_e - 1)E_z(x,y,o)\vec{a}_z \quad \ldots(2.24)$$

---

* The expression used to evaluate ϵ_e is given on page 22.

c) The total current density is:

$$\vec{J}_T = \vec{J}_{CR} + \vec{J}_{CI} + \vec{J}_P \qquad \ldots(2.25)$$

$$\vec{J}_T = \left\{ - H_y(x,y,h) + H_y(x,y,-h) \right\} \vec{a}_x + \left\{ H_x(x,y,h) - H_x(x,y,-h) \right\} \vec{a}_y + \left\{ j\frac{k}{120\pi} (\varepsilon_e - 1) E_z(x,y,o) \right\} \vec{a}_z \qquad \ldots(2.27)$$

The above expression will be used to derive the radiation properties of the triangular resonator.

CHAPTER III

RADIATION PROPERTIES OF THE TRIANGULAR RESONATOR

3.1 INTRODUCTION

Two different methods can be used to derive the expression for the radiated power from a microstrip structure. The first is the waveguide approach where the geometry of the structure defines the aperture which radiates into the hemisphere above the ground plane. In the above case the field distribution at the aperture must be known. The second method considers the structure as an antenna with a known current distribution. Either approach requires certain simplifying assumptions, the validity of which determines the accuracy of the theoretical results. In the following analysis, knowing the current distribution in the triangular structure, the antenna approach is used.

3.2 FAR ZONE ELECTRIC FIELD COMPONENTS:

The expression for the Hertz vector (2.15), in the case of a structure radiating into the free space is,

$$\vec{\Pi} = \frac{-j}{4\pi}\sqrt{\frac{\mu_o}{\varepsilon_o}}\,\frac{1}{k}\int_{\tau}\frac{e^{-jkr}}{r}\,\vec{J}\,d\tau \qquad \ldots(3.1)$$

After substituting r with the approximate expression derived for the far-field zone (Appendix A):

$$\vec{\Pi} = \frac{-j}{4\pi}\sqrt{\frac{\mu_o}{\varepsilon_o}}\ \frac{1}{k}\ \int_\tau \frac{e^{-jk\left(r_o - \frac{x_o}{r_o}x - \frac{y_o}{r_o}y - \frac{z_o}{r_o}z\right)}}{r_o\left(1 - \frac{x_o}{r_o^2}x - \frac{y_o}{r_o^2}y - \frac{z_o}{r_o^2}z\right)}\ \vec{J}\ d\tau \qquad \ldots(3.2)$$

Neglecting the second order terms in the denominator and substituting $\frac{1}{120\pi}$ instead of the intrinsic wave impedance $\sqrt{\frac{\varepsilon_o}{\mu_o}}$, the Hertz vector is further simplified.

$$\vec{\Pi} = -j\frac{30}{k}\frac{e^{-jkr_o}}{r_o}\ \int_\tau e^{\,jk\left(\frac{x_o}{r_o}x + \frac{y_o}{r_o}y + \frac{z_o}{r_o}z\right)}\ \vec{J}\ d\tau \qquad \ldots(3.3)$$

This integration is carried out in Appendix B. The result of the integration being independent of x, y and z, the electric field vector (2.16) can be simplified:

$$\vec{E} = k^2\ \mu_r\ \varepsilon_r\ \vec{\Pi} \qquad \ldots(3.4)$$

where $\mu_r = \varepsilon_r = 1$

The coordinate transformation described in Appendix A is then applied to (3.4) and after equating to zero the radial component of the

electric field vector as the definition of the far-field approximation requires, the following expressions are obtained.

$$\left.\begin{aligned} E_r &= 0 \\ E_\theta &= k^2 \left(\Pi_x \cos\theta \cos\phi + \Pi_y \cos\theta \sin\phi - \Pi_z \sin\theta\right) \\ E_\phi &= k^2 \left(-\Pi_x \sin\phi + \Pi_y \cos\phi\right) \end{aligned}\right\} \quad \ldots(3.5)$$

3.3 RADIATED POWER:

The time rate of energy flow per unit area, for a radiating element, is the Poynting vector or power density. The average Poynting vector is

$$\vec{P} = \tfrac{1}{2} \operatorname{Re} (\vec{E} \times \vec{H}^*) \quad \ldots(3.6)$$

where E, H are peak values

and $\vec{H}^*$ is the complex conjugate of $\vec{H}$. The far-zone radiation assumes that the field vectors have only real components, therefore noticing that

$$\vec{H}^* = \sqrt{\frac{\epsilon_o}{\mu_o}} \; \vec{E}^* \quad \ldots(3.7)$$

the average radiated power is expressed as:

$$P_r = \frac{1}{2} \sqrt{\frac{\epsilon_o}{\mu_o}} \iint |\vec{E}|^2 \; ds \quad \ldots(3.8)$$

The above expression is a scalar quantity and can be rewritten

for this particular case as:

$$P_r = \frac{1}{2} \sqrt{\frac{\epsilon_o}{\mu_o}} \int_o^{2\pi} \int_o^{\pi/2} \left(E_\theta^2 + E_\phi^2\right) r^2 \sin\theta d\theta d\phi \quad ....(3.9)$$

Numerical method can be used to evaluate (3.9) but they do not lead to an absolute result since the arbitrary amplitude factor $(A_{1,0,-1})^2$ will be involved. This is avoided by calculating the radiation quality factor, Q_r. This factor is defined as follows:

$$Q_r = \frac{\omega_o \cdot \text{Energy stored in the circuit}}{\text{Average power radiated}} \quad ....(3.10)$$

Another quantity which is often used is the fraction of the stored power which is radiated.

$$P_{\text{radiated}} \left[\text{in } \%\right] = \frac{1}{Q_r} \times 2\pi \times 100\% \quad ....(3.11)$$

3.4 NUMERICAL RESULTS:

A computer program was written (Appendix C) to calculate the radiation Q using the expression (3.10). Some of the computed results are given in Table 3.1. The effective dielectric constant used in the program was calculated from Schneider's [1] expression.

$$\epsilon_e \approx \frac{\epsilon_r + 1}{2} + \frac{\epsilon_r - 1}{2} \cdot \left(1 + \frac{10h}{w}\right)^{-\frac{1}{2}} \text{ with } t = 0 \quad ....(3.12)$$

where w is the width of the microstrip

h is the thickness of the microstrip

t is the thickness of the metallization

Although the width of the structure is variable, the effective permittivity was assumed to be constant in order to simplify the calculations. ε_r was taken to be the value corresponding to the width of the triangle at the origin of the x-y coordinates system.

In Fig. 3.1, the computed values for Q_r^{-1} are plotted against h.f, where f is the resonant frequency associated with the fundamental mode. As it is shown below, the relationship between the inverse of the radiation Q and the product h.f is linear.

From expression (2.13), $a \propto f^{-1}$

and $k = \frac{2\pi}{\lambda}$ implies, $k \propto f$

from Appendix C, for small $\left(\frac{k Z_o h}{r_o}\right)$, $\vec{\Pi} \propto h.f^{-1}$

thus from (2.31), $\vec{E} \propto h$

and from (2.14), $W_{stored} \propto h.f^{-2}$

therefore from (3.8), $Q_r \propto (h.f)^{-1}$

3.5 CONCLUSION OF THE THEORETICAL ANALYSIS

The results of the theoretical analysis show that the power radiated from the triangular structure is proportional to the product of thickness of the dielectric material and the resonance frequency.

A(mm)	h(mm)	ε_r	f(GHz)	ε_e	$P_r \times 10^9$ (w)	Stored Energy $x f x 10^9$ (w)	% P_r	Q_r	$h x f x 10^7$
15.2	1.27	1	13.12	1	5.5	11.1	50	13	1.67
20.3	1.27	1	9.84	1	5.6	14.9	38	17	1.25
15.2	0.64	1	13.12	1	1.4	5.5	25	25	.83
20.3	0.64	1	9.84	1	1.4	7.4	19	33	.63
10.2	1.52	2.5	12.45	2.15	4.1	14.1	29	22	1.90
12.7	1.52	2.5	9.96	2.18	4.2	17.6	24	27	1.52
15.2	1.52	2.5	8.30	2.20	4.2	21.1	20	31	1.26
20.3	1.52	2.5	6.22	2.24	4.3	28.1	15	41	.95
10.2	0.76	2.5	12.45	2.24	1.1	7.0	15	41	.95
12.7	0.76	2.5	9.96	2.28	1.1	8.8	12	51	.76
15.2	0.76	2.5	8.30	2.30	1.1	10.6	10	61	.63
20.3	0.76	2.5	6.22	2.33	1.1	14.1	8	80	.47
5.1	1.52	10	12.45	7.31	1.2	14.1	9	72	1.90
6.4	1.52	10	9.96	7.48	1.3	17.6	7	88	1.52
7.6	1.52	10	8.30	7.63	1.3	21.1	6	103	1.26
10.2	1.52	10	6.22	7.87	1.3	28.1	5	140	.95
5.1	1.27	10	12.45	7.45	.87	11.7	7	84	1.58
6.4	1.27	10	9.96	7.63	.89	14.7	6	103	1.26
7.6	1.27	10	8.30	7.78	.91	17.6	5	122	1.05
10.2	1.27	10	6.22	8.03	.93	23.4	4	158	.79
5.1	0.64	10	12.45	8.03	.23	5.9	4	158	.79
6.4	0.64	10	9.96	8.22	.24	7.3	3	194	.63
7.6	0.64	10	8.30	8.37	.24	8.8	3	228	.53
10.2	0.64	10	6.22	8.62	.25	11.7	2	299	.40

Table 3.1 - Computed radiation data for the triangular resonator

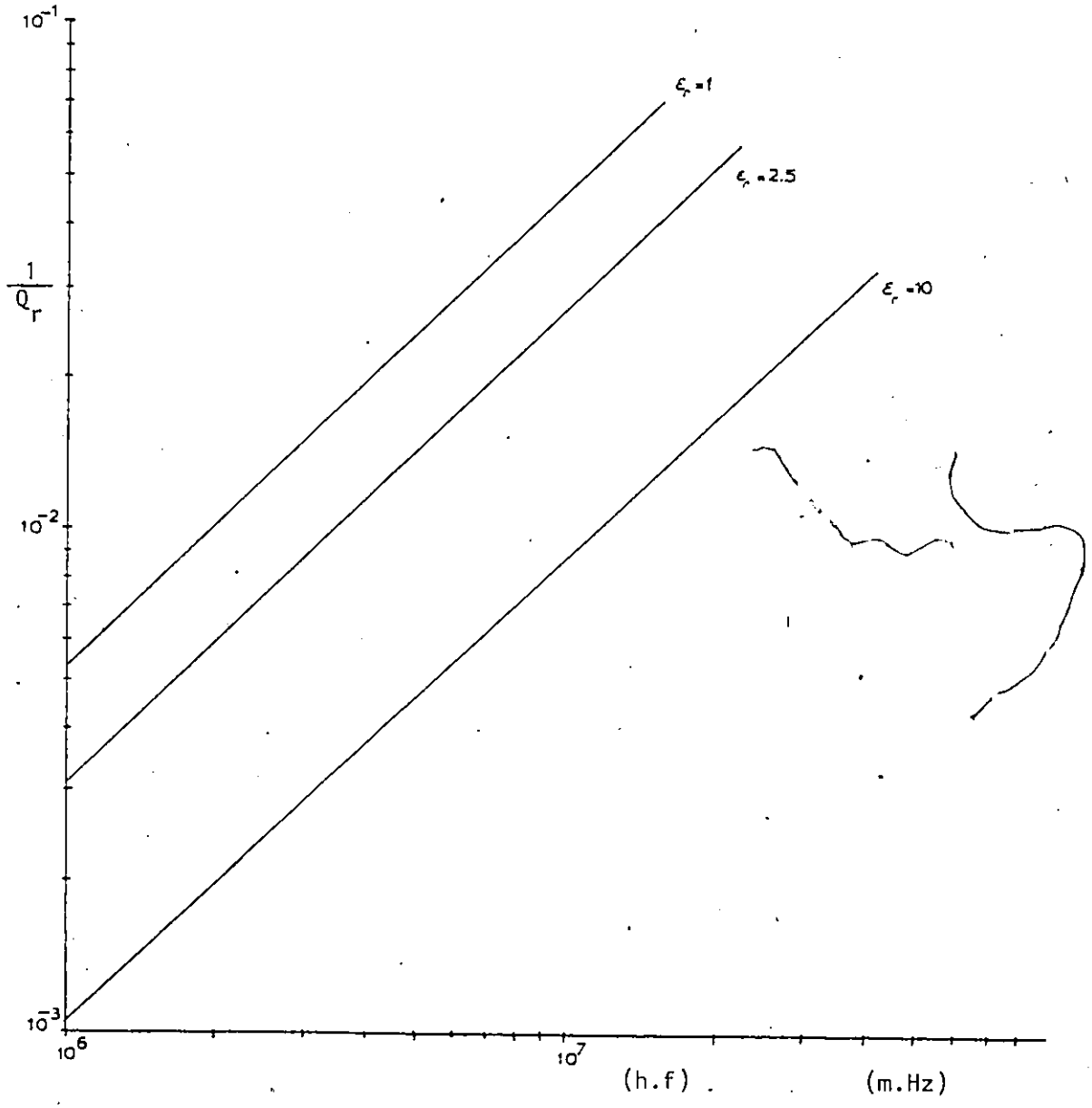

Fig. 3.1 - Q_r^{-1} versus the product (h.f), computed results

Q_r is the radiation quality factor,

Q_r is the substrate thickness,

f is the resonance frequency

Another factor affecting the radiation is the permittivity of the substrate; a decrease in the value of the relative dielectric constant corresponds to an increase in the radiated power. The latter is shown on Fig. (3.2) where theoretically calculated values of the radiation quality factor are plotted against the relative permittivity for constant frequency of resonance and thickness of the substrate.

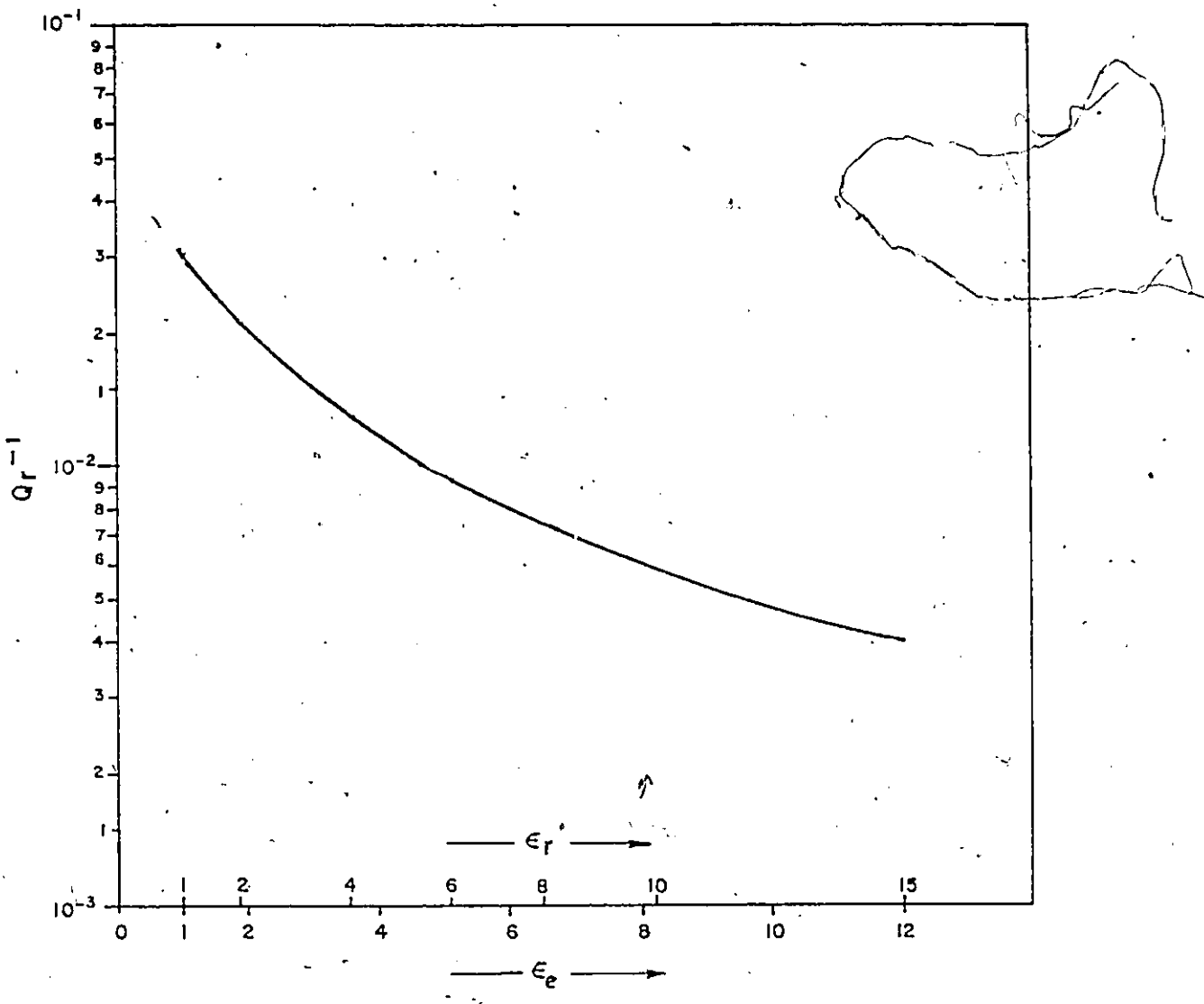

Fig. 3.2 - Computed values of Q_r^{-1} versus both relative and effective permittivity. (h=0.64mm, f=10 GHz)

CHAPTER IV

RADIATION PATTERN MEASUREMENTS

4.1 ANTENNA TEST MEASUREMENTS

The theoretical expressions and results for the power radiated from the triangular resonator, were derived in the previous Chapters, by using some approximations. A comparison of the measured field patterns with the theoretical results may be used as a first verification of the correctness of the analysis.

The experiment involved the E- and H-field pattern measurements of the triangular resonator in an anechoic chamber. The set-up, Fig. (4.1), consisted of (i) a transmitting horn antenna, (ii) the device under test (DUT) as the receiving antenna, mounted on a table whose plane can rotate around the horizontal and the vertical axis and (iii) a standard gain horn. The E- and H-plane far-field patterns were measured by rotating the DUT around an axis orthogonal and parallel to the E-field of the radiating element respectively.

The power gain of the DUT was measured by comparison with the standard gain horn. The reference gain of the standard gain horn was computed from the structures geometry.

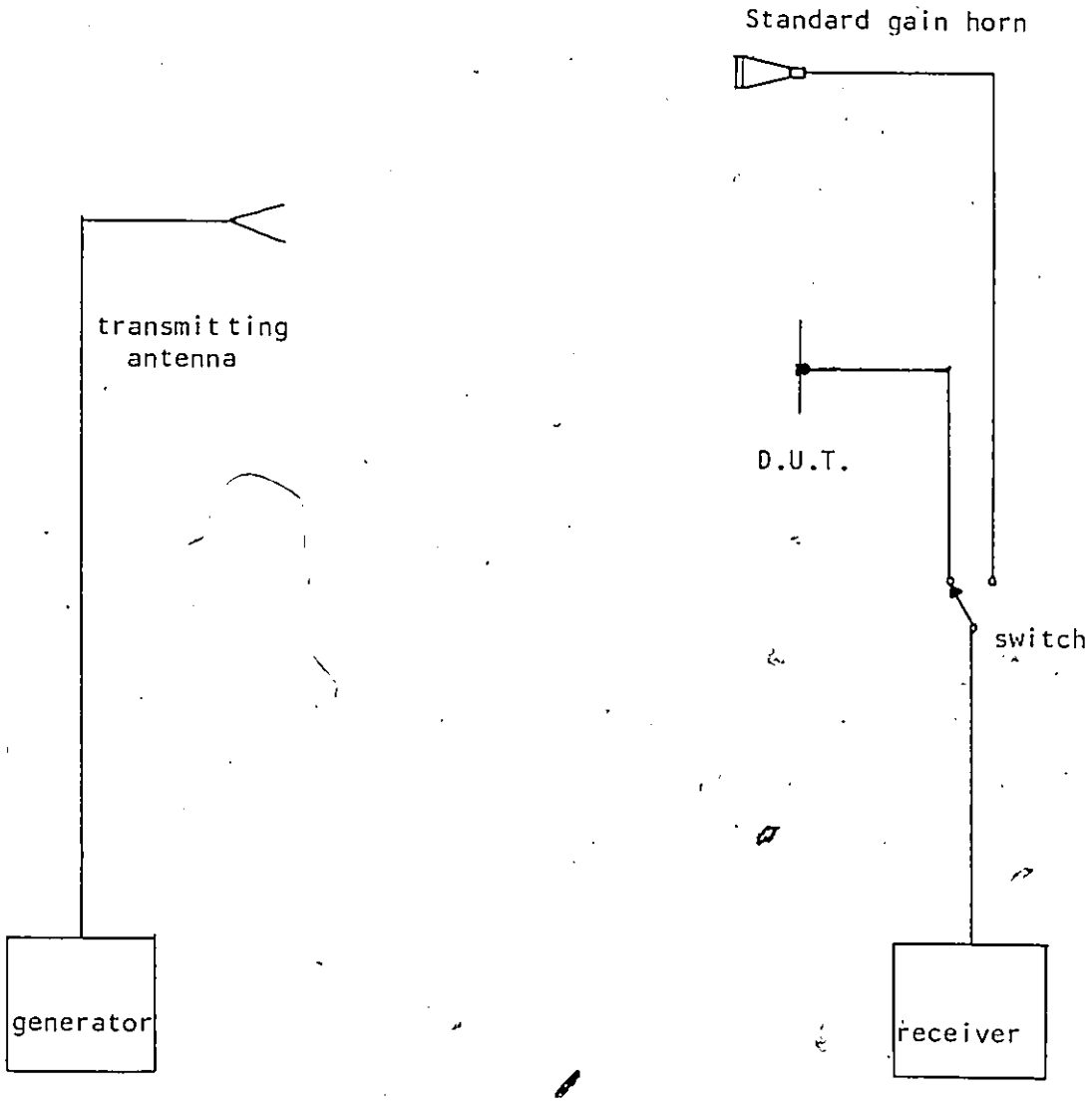

Fig. 4.1 - Set-up for radiation pattern measurement.

4.2 THEORETICAL RESULTS OF THE E- AND H-PLANE PATTERNS

The graph of the modulus of the Poynting vector, $|\vec{P}|$, at a constant distance from the radiating element, as a function of θ or ϕ is called the power pattern. This expression was derived in section (3.2) as:

$$|\vec{P}| = \frac{1}{2} \sqrt{\frac{\epsilon_o}{\mu_o}} \; |\vec{E}|^2 \qquad \ldots(4.1)$$

This can be written as:

$$|\vec{P}| = \frac{1}{2} \times \frac{1}{120\pi} \left(E_\theta^2 + E_\phi^2 \right) \qquad \ldots(4.2)$$

The expression (4.2) is solved using numerical methods by replacing the arbitrary amplitude factor $(A_{1,0,-1})^2$ with unity. The computer program is given in Appendix D. To compute the results of the E-plane pattern, the value of θ is varied from 0° to 90° in steps of 10^0 and ϕ is kept constant respectively at 0° and 180°. The H-plane pattern results are calculated for $\phi = 90^\circ$ and 270°.

4.3 THE TESTED STRUCTURES

A singly loaded triangular resonator was designed on a 1.27 mm thick alumina substrate with $\epsilon_r = 10$. The frequency of resonance was measured to be 9.6 GHz and the return loss was 15 dB which corresponds

to a VSWR of 1.43. The substrate was mounted on a 1.2 m diameter ground plane for the radiation pattern measurements. In order to lower the effect of the feed radiation, the substrate dielectric was extended around the coax to microstrip transition. The maximum measured power gain of the element was about 4.2 dB.

A second circuit was designed, this time on a 1.52 mm RT/Duroid substrate, $\varepsilon_r = 2.2$. The measured bore sight power gain was 6.5 dB.

4.4 RESULTS AND DISCUSSION

The results of the measured and theoretical radiation patterns for the resonator, on an alumina substrate, are compared in Figures 4.2, 4.3, 4.4 and 4.5. The theoretical results are normalized to the corresponding maximums of the measured radiation patterns. It can be seen that the theory underestimates the radiation. As an antenna element, the resonator has a wide half-power beamwidth which is the case for most of the microstrip single antenna structures. Also, because the cross-polarization is low, the triangular element is essentially linearly polarized.

The power gain measurements show that the lower the relative dielectric constant of the substrate, the more the antenna element radiates, as was expected from the theory.

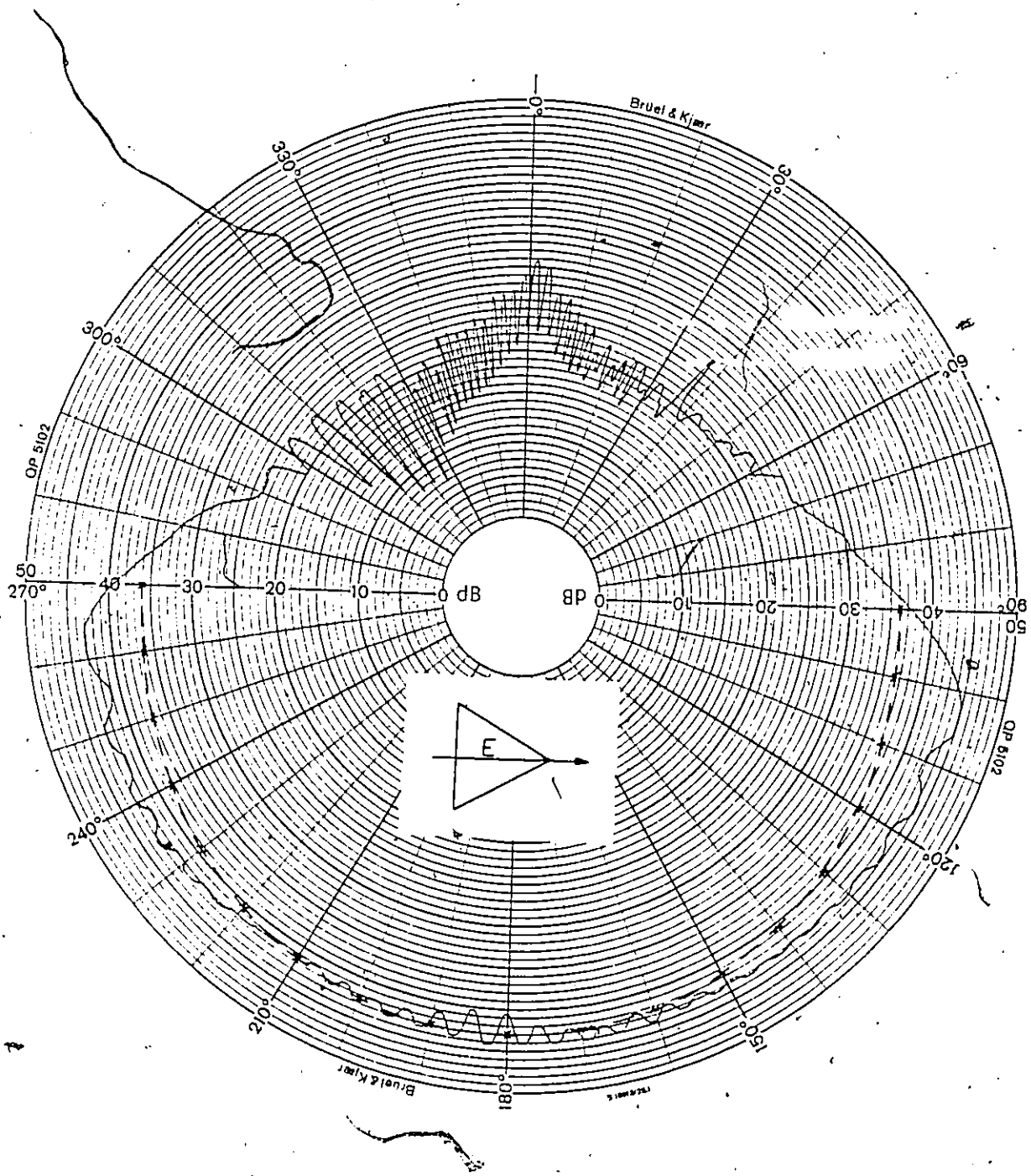

Fig. 4.2 - Triangular resonator theoretical and experimental E-plane radiation pattern. (ε_r = 10, h = 1.27 mm, f = 9.6 GHz)

——————— measured pattern
— — — — calculated pattern

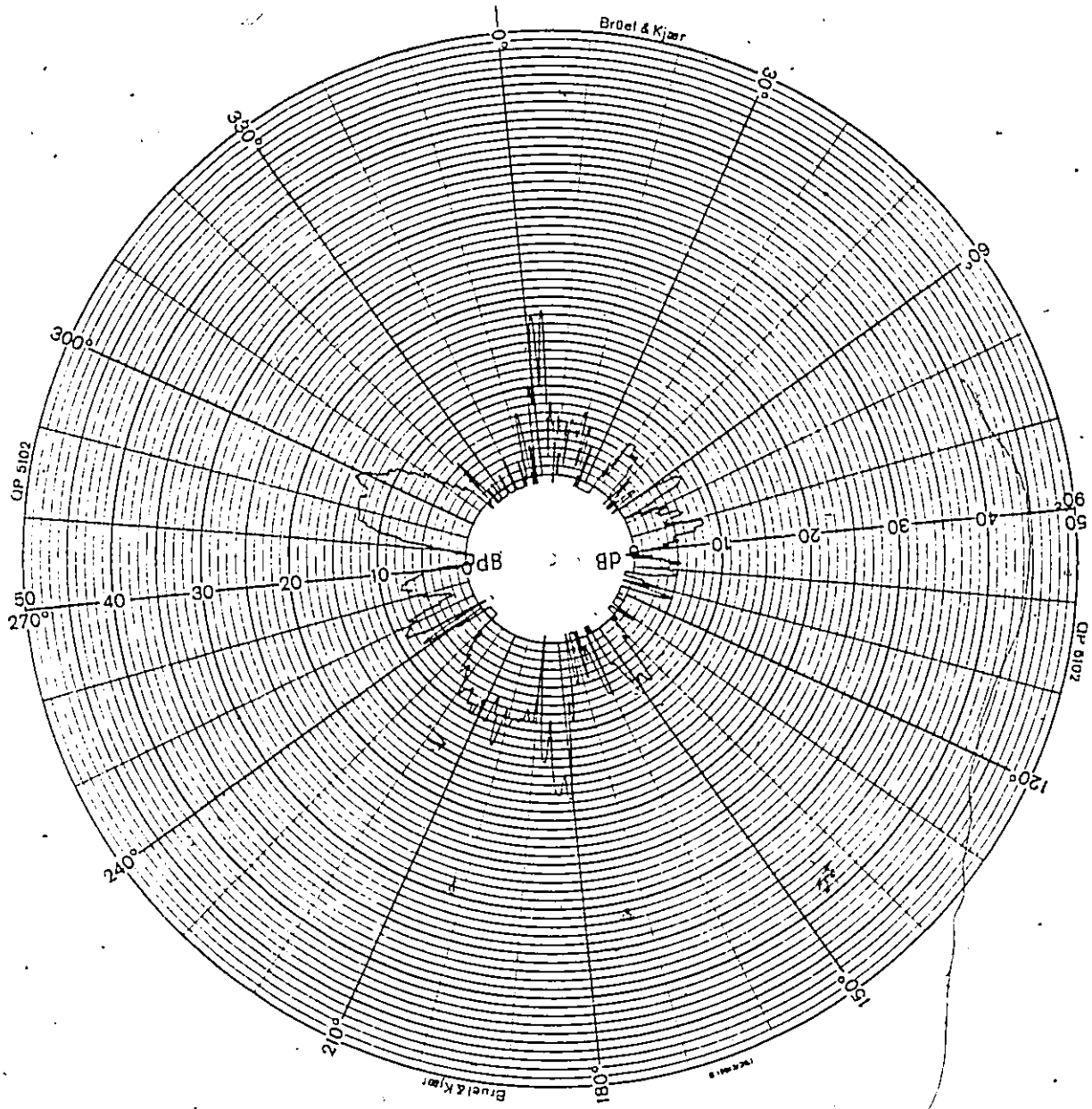

Fig. 4.3 - E-plane cross-polarization pattern
(for the same substrate as in Fig. 4.2)

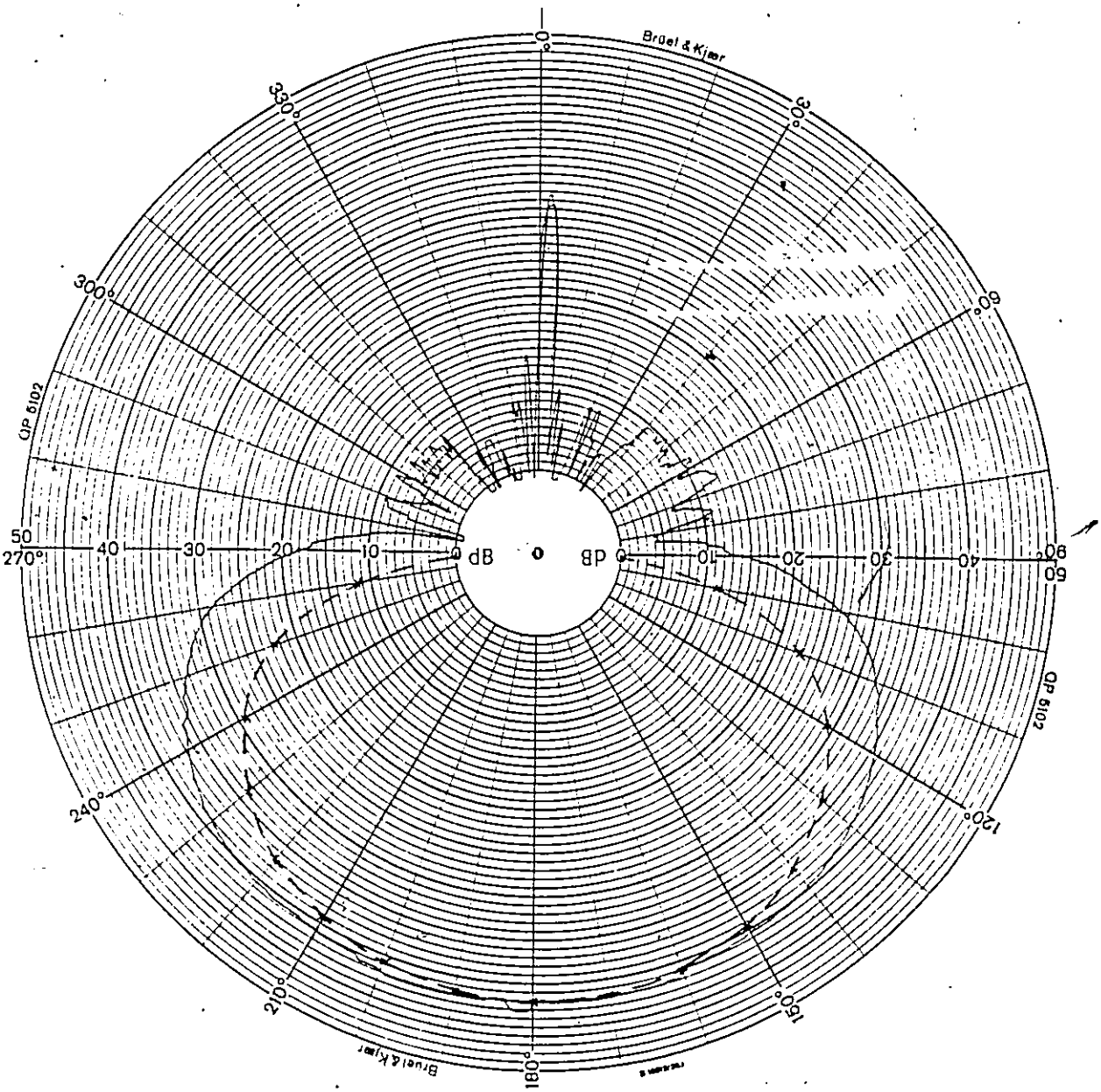

Fig. 4.4 - Triangular resonator theoretical and experimental H-plane pattern. (for the same substrate as in Fig. 4.2).

——— measured pattern

— — — theoretical pattern

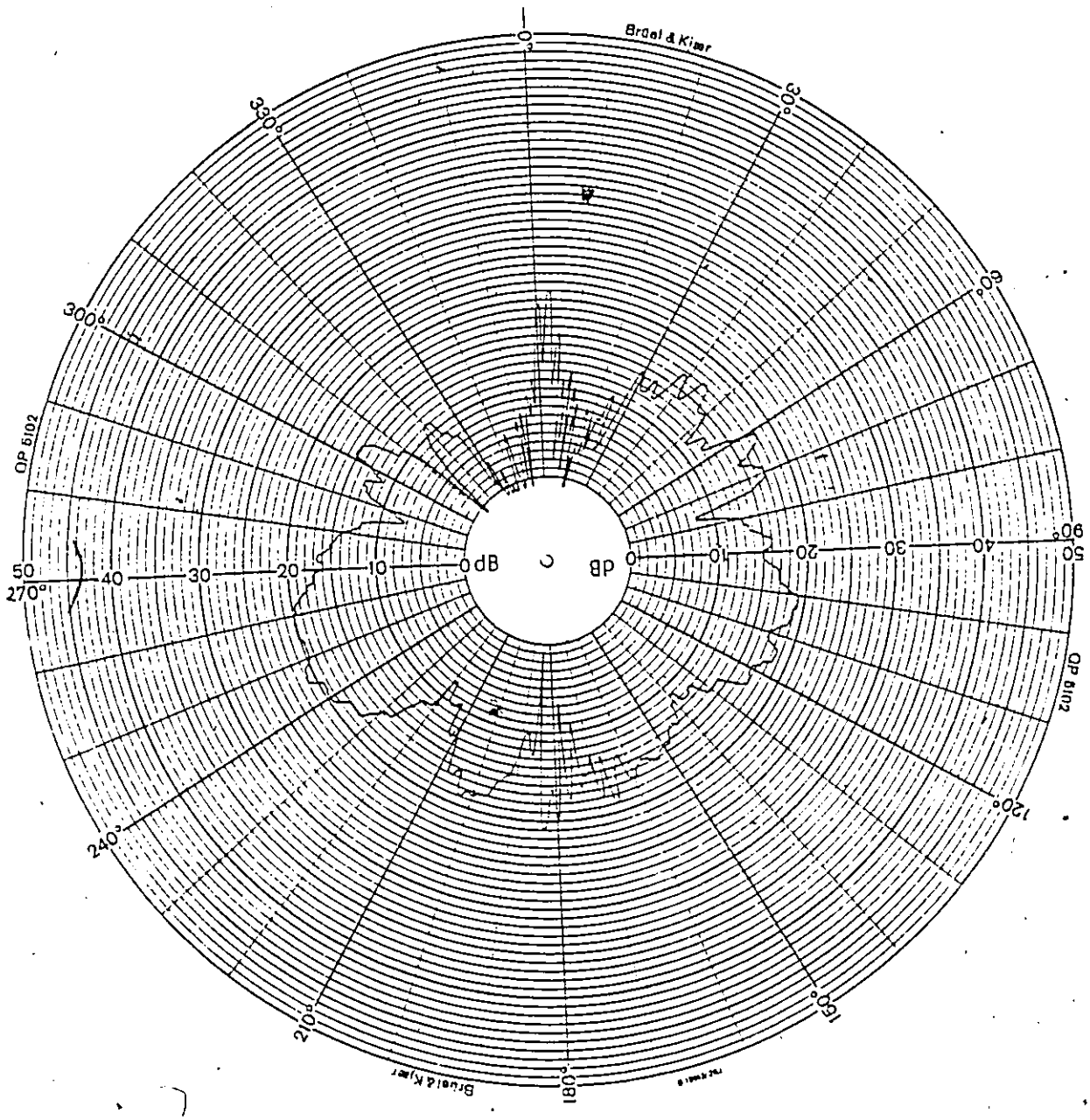

Fig. 4.5 - H-plane cross-polarization pattern.
(for the same substrate as in Fig. 4.2).

CHAPTER V

RADIATION QUALITY FACTOR MEASUREMENTS

5.1 DEFINITION OF THE QUALITY FACTOR

The losses in a resonant cavity determine its quality factor, Q. A perfect resonator, without any coupling, dielectric, resistive or radiation losses would have a Q of infinity. Mainly three different Q's - the unloaded, the loaded and the external Q - are used in the analysis of a cavity and its peripherial circuits.

For the unloaded Q, Q_o, consider the energy dissipated at resonance in the cavity alone [17]:

$$Q_o = \left. \frac{\text{Energy stored in cavity}}{\text{Energy dissipated in cavity per radian}} \right| \text{at resonance}$$

The dissipated energy depends, besides the cavity mode, on one or more of the following losses, (i) the resistivity of the walls, (ii) the dielectric losses and (iii) the radiation. The unloaded Q of a 4 GHz waveguide cavity is greater than 10,000 but in the case of microstrip resonators, Q_o is only of the order of a few hundreds.

A cavity is usually coupled to a matched transmission line, and because of the loading effect of the line, the overall Q of the circuit

is lower than Q_o. The loaded Q, Q_L, is defined as:

$$Q_L = \left. \frac{\text{Energy stored in cavity}}{\text{Energy dissipated in both cavity and external circuit per radian}} \right| \text{at resonance}$$

The loaded and unloaded Q are related to each other by the means of the external Q, Q_e. This relation may be expressed as:

$$\frac{1}{Q_L} = \frac{1}{Q_o} + \frac{1}{Q_e} \qquad \ldots(5.1)$$

The definition of Q_e is:

$$Q_e = \left. \frac{\text{Energy stored in cavity}}{\text{Energy dissipated in external circuit per radian}} \right| \text{at resonance}$$

If the cavity is loaded at two points, then expression (5.1) can be modified to:

$$\frac{1}{Q_L} = \frac{1}{Q_o} + \frac{1}{Q_{e_1}} + \frac{1}{Q_{e_2}} \qquad \ldots(5.2)$$

5.2 LOSSES IN MICROSTRIP RESONATORS

Microstrip structures have low Q factors due to the high losses. The unloaded Q of a microstrip is expressed by the sum of three main losses.

$$\frac{1}{Q_o} = \frac{1}{Q_\varepsilon} + \frac{1}{Q_c} + \frac{1}{Q_r} \qquad \ldots(5.3)$$

where: Q_ε is a measure of the dielectric losses

Q_c is a measure of the conductor losses

Q_r is a measure of the radiation losses

Q_ε is inversely proportional to the loss tangent of the dielectric material. For alumina substrates, with relative dielectric constant, ε_r, of approximately 10, the loss tangent is of the order of 10^{-4} up to 10 GHz. For RT/Duroid 5880, $\varepsilon_r = 2.2$, the loss tangent is of the order of 10^{-3}. The surface roughness of the dielectric also contributes to the dielectric losses. In order to account for these losses Q_ε must be divided by a factor of 1.04 in the case of alumina substrates at 8 GHz, and by 1.8 in the case of RT/Duroid 5880 [12].

The conductor losses can be calculated using a simple analysis which does not include the effects of fringing fields and radiation [6]. Q_c can be expressed as:

$$Q_c = (\pi \mu_o f \sigma)^{\frac{1}{2}} h \qquad \ldots.(5.4)$$

where: σ is the conductivity in $^S/_m$

h is the substrate thickness in m

f is the frequency in Hz

μ_o is $4\pi \times 10^{-7}\ ^H/_m$

For copper ($\sigma = 5.9 \times 10^7\ ^S/_m$), at 10 GHz, on a 0.635 mm thick substrate,

$$Q_c \sim 969$$

For bulk gold, ($\sigma = 4.55 \times 10^7$ $^S/_m$)

$$Q_c \quad 851$$

From literature it is known that radiation losses depend on the geometry of the structure [8,10]. Therefore, neglecting dielectric and conductor losses and assuming that radiation is the dominant source of losses cannot be justified for all cases, since Q_r is of the order of a few hundreds.

5.3 THE QUALITY FACTOR MEASUREMENT

The Q of a resonator can be found by measuring the bandwidth between the half-power frequencies when the circuit is excited by a constant current source.

$$Q = \frac{f_o}{\Delta f} \qquad \ldots.(5.5)$$

where: f_o is the center frequency,

$\Delta f = f_2 - f_1$, is the half-power bandwidth

The measurement will give the loaded Q, Q_L, which will lead to Q_o after a simple calculation, provided the input and output coupling are made equal.

If the input and output coupling coefficients between the cavity and the external circuit are β_1, and β_2 respectively, then (18)

$$Q_L = \frac{Q_o}{1 + \beta_1 + \beta_2} \qquad \ldots.(5.6)$$

and the transmitted power factor at resonance is:

$$\tau_{res} = \frac{4\beta_1\beta_2}{(1 + \beta_1 + \beta_2)^2} \qquad \ldots.(5.7)$$

For $\beta_1 = \beta_2 = \beta$, the expressions (5.6) and (5.7) become,

$$Q_L = \frac{Q_o}{(1 + 2\beta)} \qquad \ldots.(5.8)$$

$$\tau_{res} = \frac{4\beta^2}{(1 + 2\beta)^2} \qquad \ldots.(5.9)$$

Respectively, it is also interesting to note that the transmitted power is maximum for $\beta_1 = \beta_2$

The expression (5.8) can be rewritten as:

$$1 - \frac{Q_L}{Q_o} = \frac{2\beta}{1 + 2\beta} \qquad \ldots.(5.10)$$

Which leads to:

$$\tau_{res} = \left(1 - \frac{Q_L}{Q_o}\right)^2 \qquad \ldots.(5.11)$$

$$Q_o = \frac{Q_L}{1 - \sqrt{\tau_{res}}} \qquad \ldots.(5.12)$$

Thus it can be seen from expression (5.12) that a transmission loss measurement at the resonant frequency and a knowledge of the half-power bandwidth of the resonator will lead to the unloaded Q. It should also be noted that Q_L approaches Q_o as the coupling between the cavity and the external circuit becomes looser.

5.4 THE RADIATION Q MEASUREMENT TECHNIQUE

A direct measurement of Q_r, as can be seen from the expression (5.3), may involve quantities such as the resistivity of the microstrip deposition, the loss tangent of the dielectric etc. which are difficult to measure. A practical method that overcomes the above problem consists of two identical measurements; in the first measurement, the resonator is in the open, i.e. radiating. Then the resonator is placed into a shielding box with highly conducting walls. The dielectric and conductor losses being the same, it follows that,

$$\frac{1}{Q_r} = \frac{1}{Q_o} - \frac{1}{Q_s} \qquad \ldots.(5.13)$$

Where, Q_s is the shielded Q which assumes no radiation.

The dimensions of the shielding box which can be considered as a rectangular waveguide cavity should be such that it will not sustain any box modes at the frequencies of interest.

For the fundamental mode in a rectangular cavity, TE_{101}, the resonant frequency is (19):

$$f = \frac{c\sqrt{a^2 + d^2}}{2\,ad} \qquad \ldots.(5.14)$$

where: a is the width of the box

d is the length of the box

c is the speed of light in the vacuum

Fig. (5.1) shows a jig and a shield arrangement used for the experiments. They are made of solid brass blocks and held together by four screws.

5.5 EXPERIMENTAL ARRANGEMENT

Circular and triangular resonators were fabricated on alumina with $\varepsilon_r \sim 10$, h = .635 mm and h = 1.27 mm; Custom - k with $\varepsilon_r \sim 10$, h = 1.52 mm; and Rexolite with $\varepsilon_r \sim 2.5$, h = .76 mm and h = 1.52 mm substrates. The conductor layer is 4 μm thick gold in the case of alumina substrates and 25.4 μm thick copper for the other two substrates.

The designs were made such that the resonant frequency of the elements would be in the range 6 to 12 GHz. The theoretical expressions used to determine the center frequency are:

a) For the circular disc [6], $f = 1.84118 \dfrac{c}{\pi\sqrt{\varepsilon_r}\,D}$ .....(5.15)

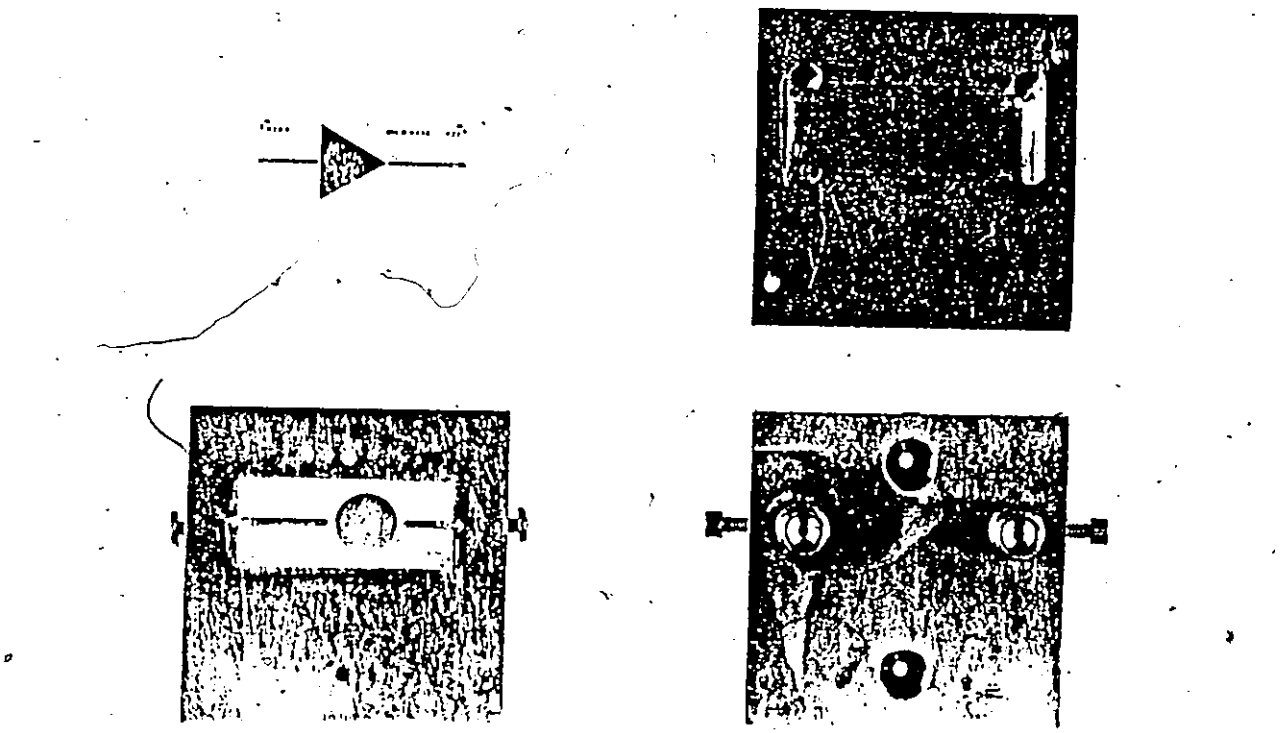

Fig. 5.1 - Jig and its cover used in Q_r measurements

b) For the triangle [2], $f = \frac{2c}{3A\sqrt{\epsilon_r}}$ ....(5.16)

where: D is the diameter of disc

A is the side of triangle

The resonators were coupled through a gap to a 50 Ω line. An interesting point in the above expressions is that, if in (5.15), D is replaced by $\frac{A\sqrt{3}}{2}$, the height of the triangle, then the expressions (5.15) and (5.16) are almost equal. The difference is around 3%.

The experiment consisted of a transmission loss measurement Fig. 5.2 between two frequencies swept by a generator. A reference level was set by connecting a semi-rigid coaxial cable between the detector head 'B' of the amplitude analyser and the output of the directional coupler. Then, the resonator jig, without its cover, was inserted between the coax and the directional coupler to measure the insertion loss. This technique was repeated for the shielded jig and Q_r was derived using the relations (5.5), (5.12) and (5.13). For all the measurements, the transmission loss at resonance was greater than 12 dB. Also, in order to make the simplifying assumption $\beta_1 = \beta_2$ explained in section 5.3, the return loss of each port was measured and made equal.

5.6 RESULTS AND DISCUSSION

The measured and the computed resonant frequencies are listed in Tables 5.1, 5.2 and 5.3. It can be seen that the difference between the theoretical and measured frequencies is greater for alumina than for

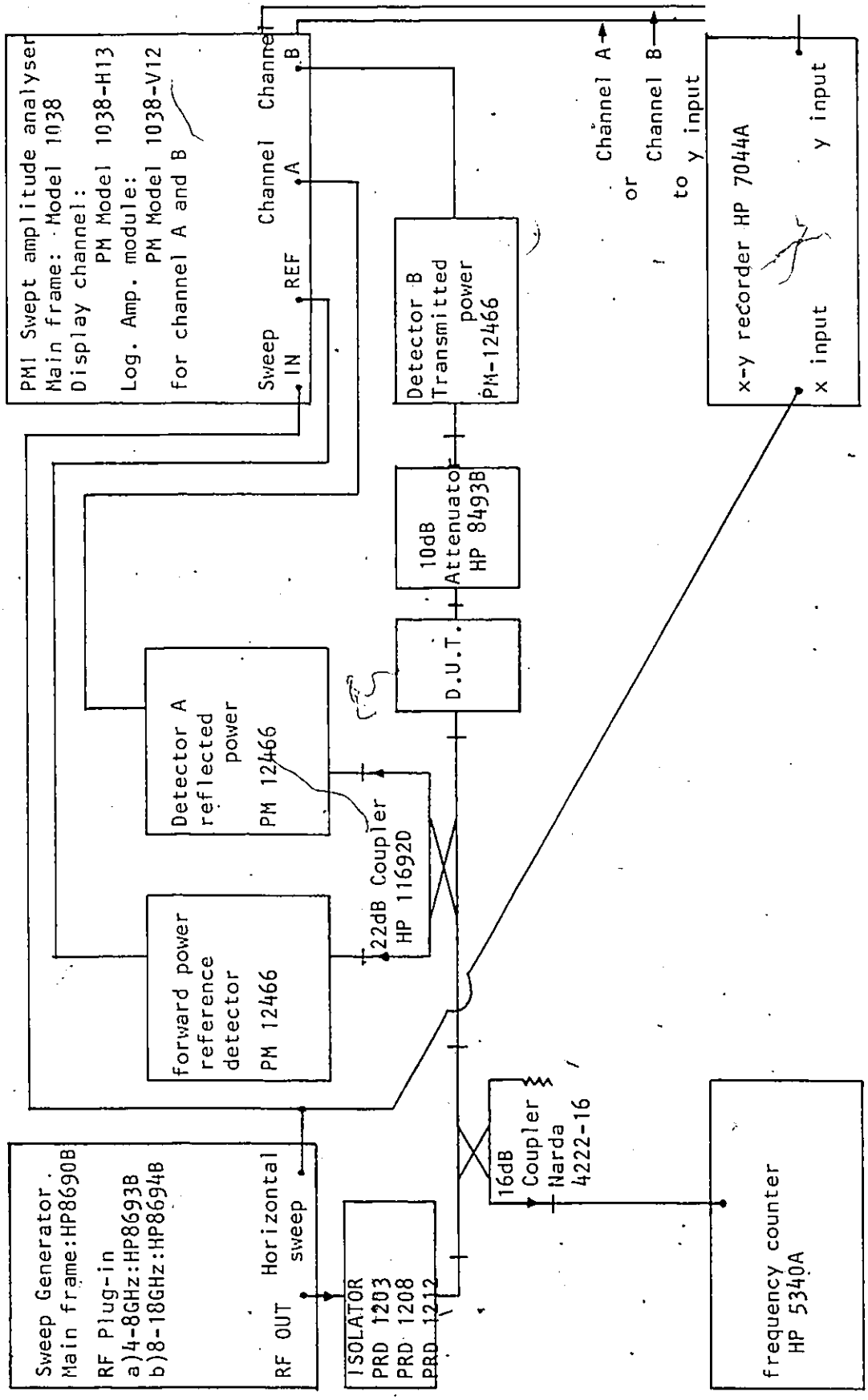

Fig. 5.2 - Set-up to measure both the reflected and the transmitted power

Custom-K even though both substrates have an $\varepsilon_r = 10$. This may be partially caused by tolerances in the dielectric constants which can be as high as ± 20% for the Custom-K material. Another possible reason for this discrepancy is that the theoretical expression for the resonant frequency does not include the effects of the fringing field. Therefore, the measured frequencies will differ if the thicknesses of the used substrates are different. For the low dielectric constant material, the theoretical frequency is closer to the measured one.

Dependence of the radiation on the substrate thickness and frequency is shown in the graphs, Fig. 5.3 and Fig. 5.4, where Q_r^{-1} is plotted against h.f. The radiation losses increase as the product h.f increases. Also as a basis for comparison, radiation from a 50 Ω quarter wave resonator as calculated by Belohoubek and Denlinger [12] is shown in Fig. 5.3. The lines drawn through the measured points have a slope close to unity, while, for the quarter wave resonator, the slope of the line is approximately 2. The latter result is expected since Lewin's analysis [4] shows that radiation from a microstrip line is proportional to $(h.f)^2$. The graphs also demonstrate that the radiation loss for circular resonators is higher than for triangular ones. The quarter wave, 50 Ω resonator radiates least among the measured structures. In general, the losses may be lowered by using thin and high dielectric constant materials.

A(mm)	h(mm)	Measured f(GHz)	Calculated f(GHz)	Q_s	Q_o	Q_r
9.40	.64	6.6	6.7	413	116	161
7.87	.64	7.7	8.0	336	92	127
5.33	.64	11.3	11.9	443	71	85
9.40	1.27	6.3	6.7	371	63	76
7.87	1.27	7.3	8.0	436	52	60
6.35	1.27	8.8	10.0	741	32	34
5.33	1.27	10.2	11.9	298	31	34
4.83	1.27	10.8	13.1	94	23	30
9.40	1.52	6.9	6.7	451	33	30
7.87	1.52	8.0	8.0	393	21	23
6.35	1.52	9.6	10.0	589	18	18

Table 5.1 - Experimental results for the triangular resonator ($\varepsilon_r = 10$)

A(mm)	h(mm)	Measured f(GHz)	Calculated f(GHz)	Q_s	Q_o	Q_r
15.24	.76	8.3	8.3	374	50	58
12.70	.76	9.9	10.0	358	38	43
15.24	.25	8.5	8.3	111	63	146
12.70	.25	10.1	10.0	124	63	128
10.16	.25	12.5	12.4	173	62	97

Table 5.2 - Experimental results for the triangular resonator ($\varepsilon_r = 2.5$)

D(mm)	h(mm)	Measured f(GHz)	Calculated f(GHz)	Q_s	Q_o	Q_r
8.13	.64	6.5	6.8	393	91	118
6.35	.64	8.3	8.8	512	79	93
4.83	.64	10.7	11.5	469	62	71
3.56	.64	14.0	15.6	270	37	43
8.13	1.27	6.1	6.8	453	53	60
7.34	1.27	6.7	7.6	551	42	45
6.35	1.27	7.6	8.8	715	39	41
4.83	1.27	9.5	11.5	322	27	29
4.32	1.27	10.4	12.9	168	22	25
8.13	1.52	6.7	6.8	406	26	28
6.35	1.52	8.3	8.8	445	19	20

Table 5.3 - Experimental results for the disc resonator (ε_r = 10)

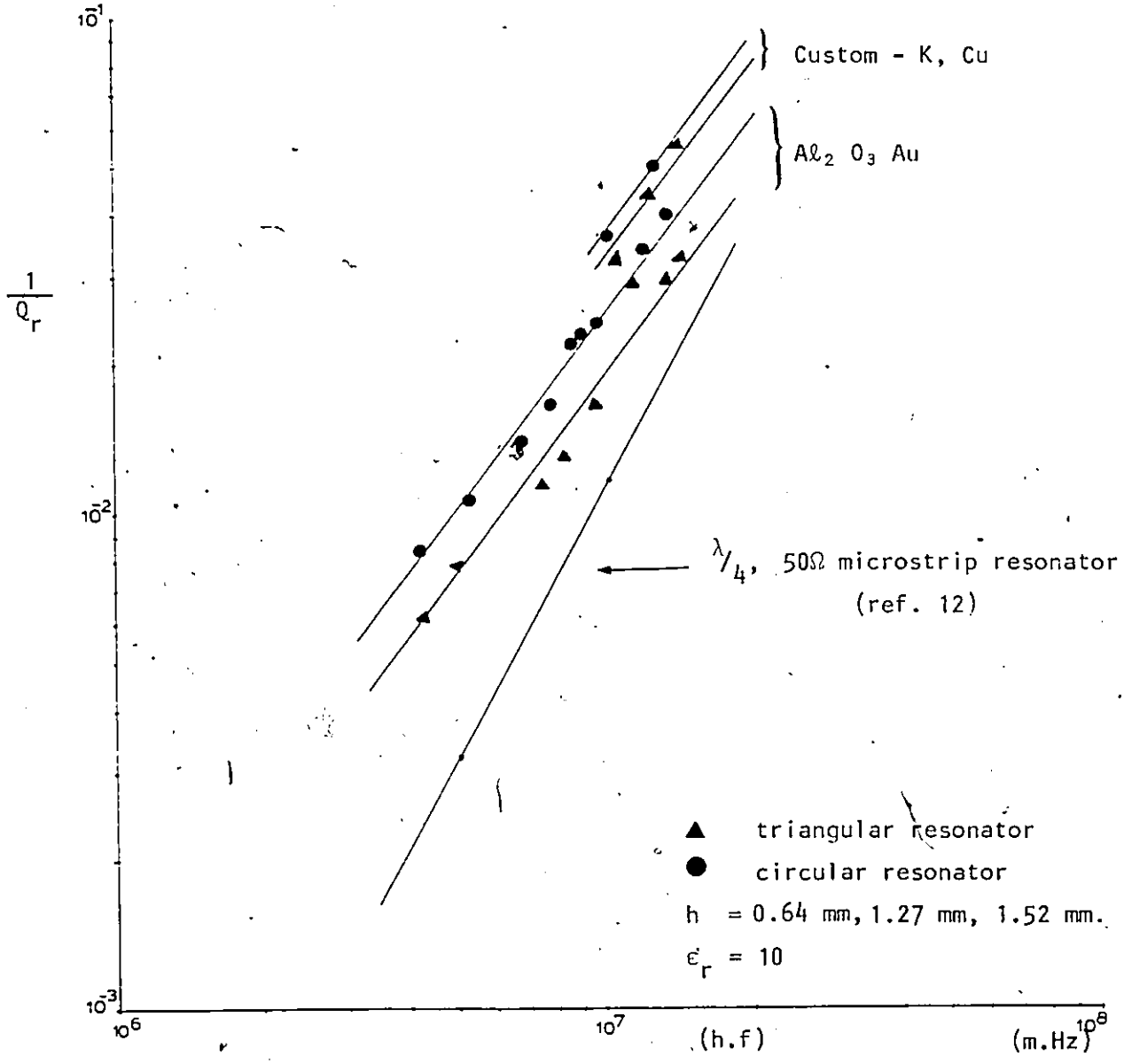

Fig. 5.3 - Measured Q_r^{-1} versus h.f for circular and triangular resonators

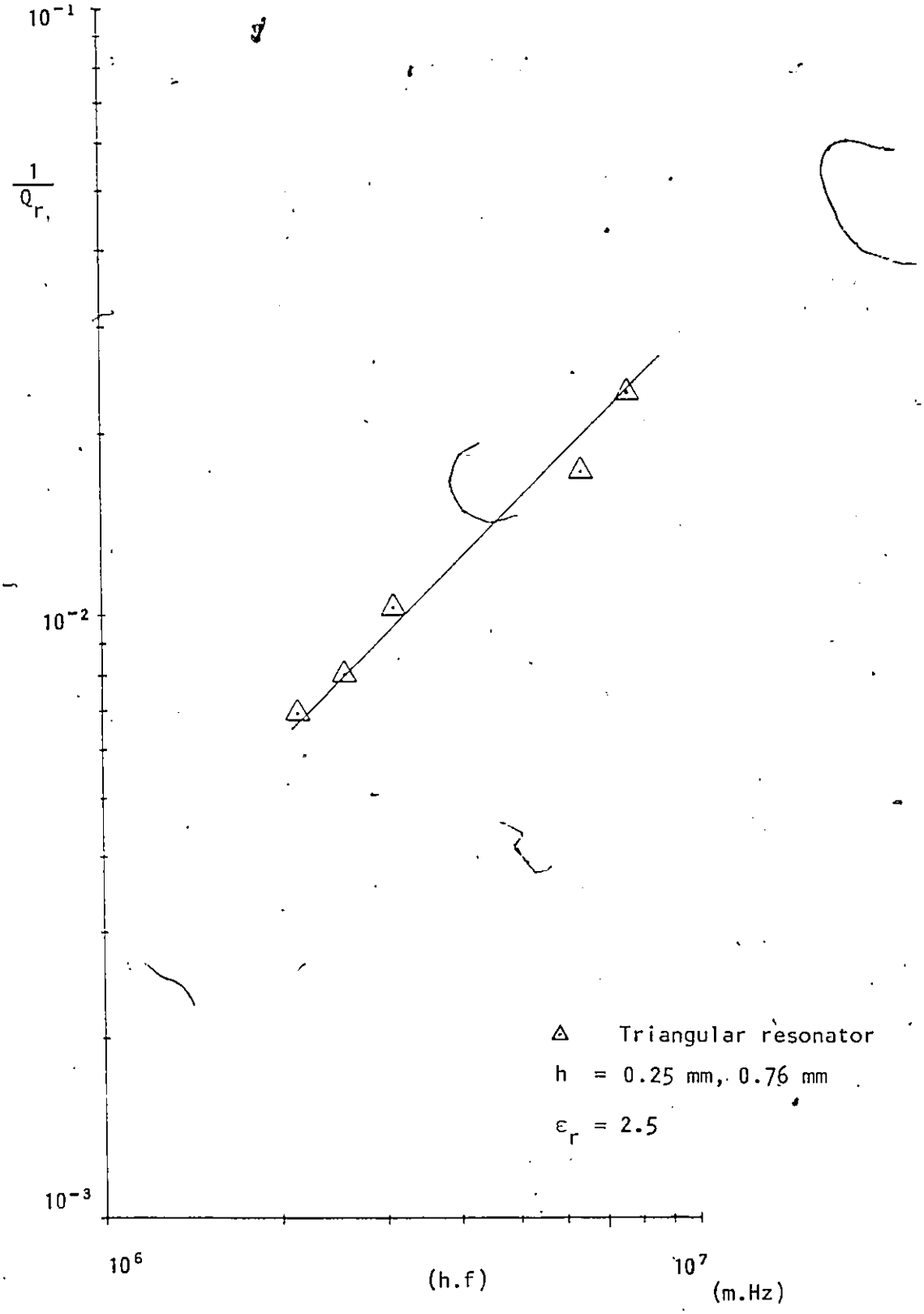

Fig. 5.4 - Measured Q_r^{-1} versus h.f for triangular resonator

CHAPTER VI

COUPLING TO A MICROSTRIP RESONATOR

6.1 COUPING TO MICROSTRIP STRUCTURES:

The radiation properties of the triangular resonator were derived assuming a very loose coupling between the resonant element and the external circuitry. Other applications, e.g. antenna measurements, may require a tight coupling. Therefore, the understanding of and the control of the energy coupled to the resonator is important.

Three types of coupling, namely capacitive, direct and hole coupling Fig. 6.1 (a,b,c) may be used with the microstrip configuration. In this Chapter, the equivalent circuit of a resonator and the coupling mechanism are studied. Some experimental gap capacitance values are also given.

6.2 EQUIVALENT CIRCUIT OF ONE PORT RESONATOR:

A one-port resonator or a reflection cavity can be represented by any of the configuration given in Fig. 6.1. The equivalent circuit of an unloaded cavity using lumped elements in parallel is shown in Fig. 6.2a. The same circuit can be modified to take into account the coupling which can be assumed to be in the form of an ideal transformer of n:1

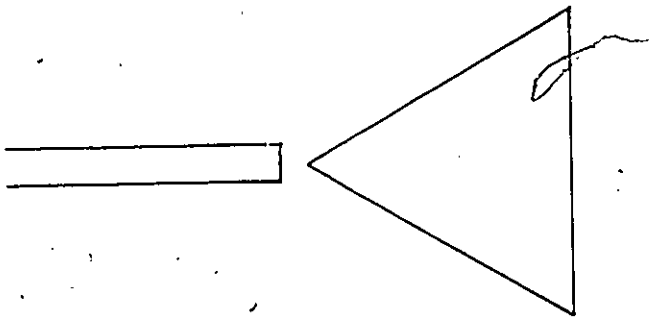

a) Capacitive gap coupling

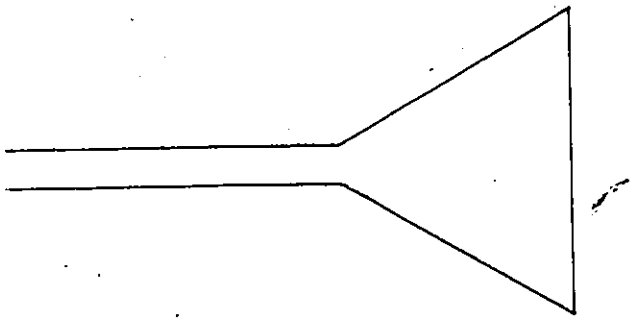

b) Direct coupling

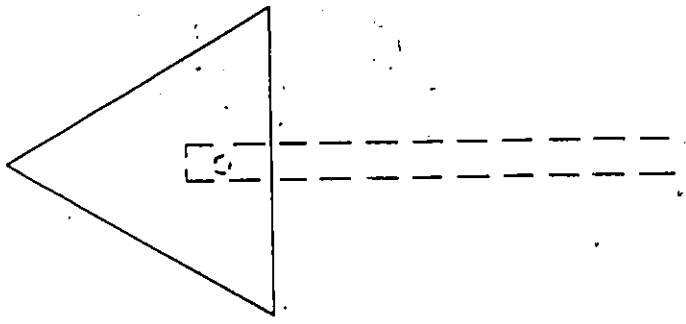

c) Hole coupling

Fig. 6.1 - Possible Microstrip coupling configurations

can be assumed to be in the form of an ideal transformer of n:1 turns ratio, the losses are incorporated in R_{eg} Fig. 6.2b [17].

The expressions,

$$R_o = n^2 R_{eg} \qquad \ldots(6.1)$$

$$L_o = n^2 L_{eg} \qquad \ldots(6.2)$$

$$C_o = \frac{C_{eg}}{n^2} \qquad \ldots(6.3)$$

represent the relationship between Fig. 6.2a and Fig. 6.2b, whereas Fig. 6.2c is obtained by normalizing the above expressions to Z_o.

The admittance of the normalized equivalent circuit is:

$$\overline{Y} = \frac{1}{\overline{R}} + j\left(\omega\overline{C} - \frac{1}{\omega\overline{L}}\right) \qquad \ldots(6.4)$$

$$\overline{Y} = \overline{G} + j\,\overline{B} \qquad \ldots(6.5)$$

with $$\omega_o = \frac{1}{\sqrt{LC}} \qquad \ldots(6.6)$$

Experimentally, n can be found from VSWR measurements.

$$|S_{11}| = \text{antilog}\left(-\frac{\text{Return loss}}{20}\right) \qquad \ldots(6.7)$$

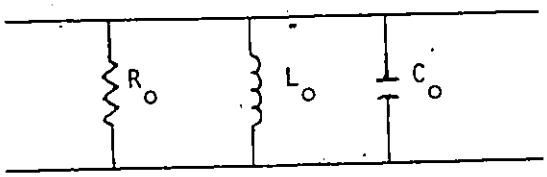

a) Cavity equivalent circuit

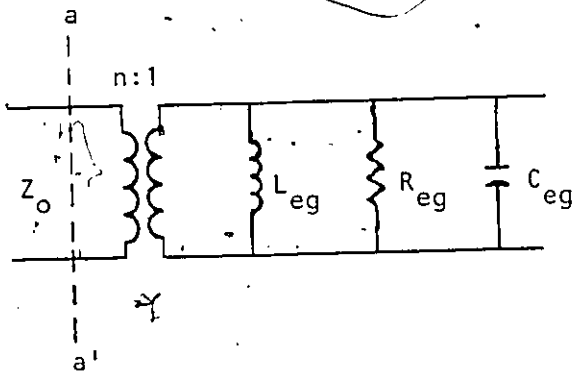

b) One port resonator equivalent circuit

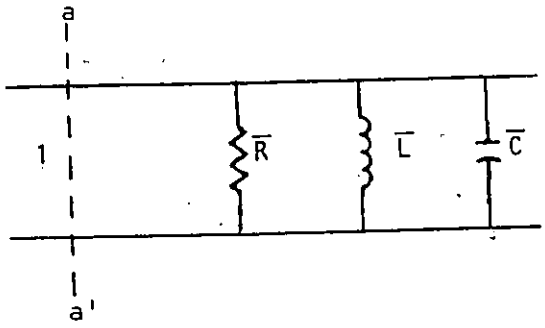

c) Normalized equivalent circuit

Fig. 6.2 - Lumped element representation of a one port cavity

and $$n^2 = \frac{1 - |S_{11}|}{1 + |S_{11}|} \qquad \ldots(6.8)$$

$\overline{G}$ can be found from the expression (6.5) after a VSWR measurement at resonance, where $\overline{B} = 0$. A second VSWR measurement close to ω_o will give $\overline{L}$ and $\overline{C}$. This can be shown after rearranging $\overline{B}$ as,

$$\overline{B} = \sqrt{\frac{\overline{C}}{\overline{L}}} \left(\frac{\omega}{\omega_o} - \frac{\omega_o}{\omega} \right) \qquad \ldots(6.9)$$

At $\omega = \omega_o + \Delta\omega$,

$$\overline{B} = \sqrt{\frac{\overline{C}}{\overline{L}}} \left(\frac{\omega_o + \Delta\omega}{\omega_o} - \frac{\omega_o}{\omega_o + \Delta\omega} \right) \qquad \ldots(6.10)$$

this expression can be represented approximately by:

$$\overline{B} \sim \sqrt{\frac{\overline{C}}{\overline{L}}} \left(\frac{2\,\Delta\omega}{\omega_o} \right) \qquad \ldots(6.11)$$

Therefore, $$\overline{L} \sim \frac{2\,\Delta\omega}{\overline{B}\,\omega_o^2} \qquad \ldots(6.12)$$

and, $$\overline{C} \sim \frac{\overline{B}}{2\,\Delta\omega} \qquad \ldots(6.13)$$

6.3 THE TWO-PORT (DOUBLE LOADED) RESONATOR EQUIVALENT CIRCUIT

The two-port resonator is a cavity with an input and output port, it is also called a transmission cavity. The equivalent circuit with ideal transformers is represented in Fig. 6.3a. The analysis of this circuit is similar to that of the one-port cavity. The output transformer is first eliminated Fig. 6.3b. Then the normalized circuit is as in Fig. 6.3c with,

$$\overline{R}' = \frac{n^2}{\overline{n}'^2} \cdot \frac{Z_o'}{Z_o} \qquad \ldots(6.14)$$

$$\overline{R} = \frac{n^2}{Z_o} R_{eg} \qquad \ldots(6.15)$$

$$\overline{L} = \frac{n^2}{Z_o} L_{eg} \qquad \ldots(6.16)$$

$$\overline{C} = \frac{Z_o}{n^2} C_{eg} \qquad \ldots(6.17)$$

The admittance of the normalized circuit is

$$\overline{Y} = \frac{1}{\overline{R}' // \overline{R}} + j\left(\omega\overline{C} - \frac{1}{\omega\overline{L}}\right) \qquad \ldots(6.18)$$

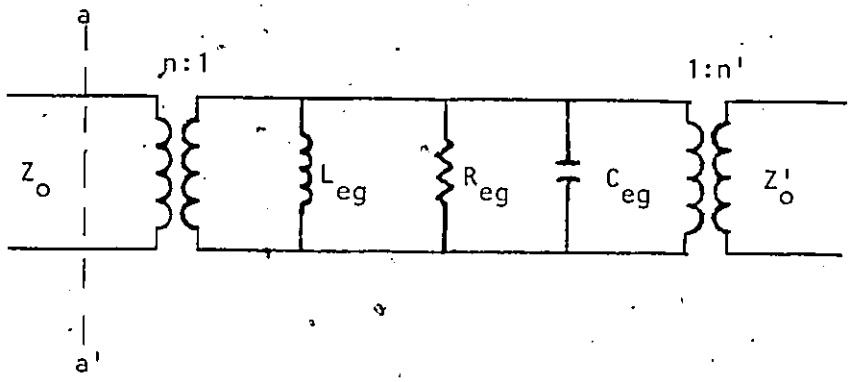

a) Two port equivalent circuit

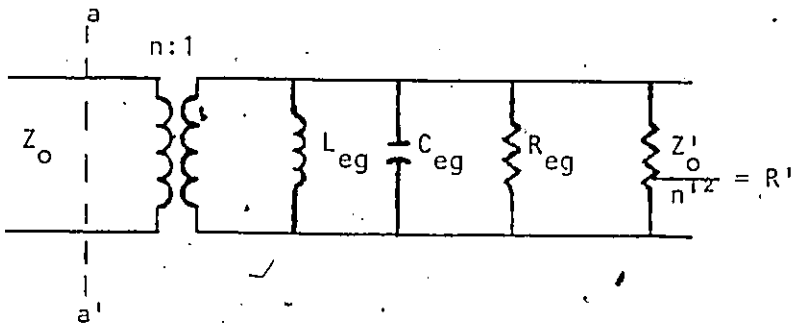

b) Without output coupling

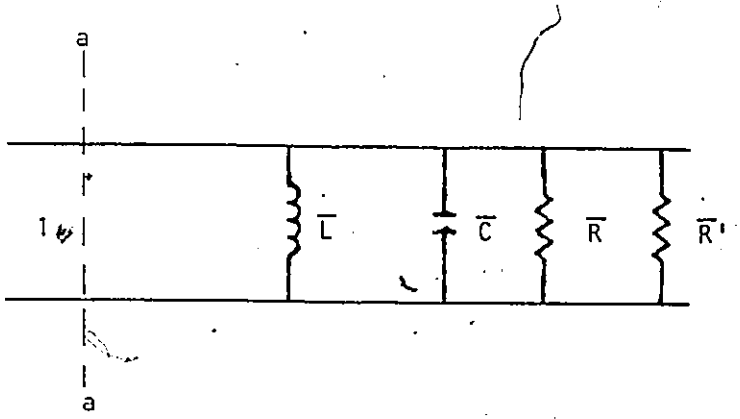

c) Normalized equivalent circuit

Fig. 6.3 - Lumped element representation of a two port cavity.

This expression differs from (6.4) only in the resistive term which is $\overline{R}'$ in parallel with $\overline{R}$.

$$\overline{R}' \,//\, \overline{R} = \frac{\overline{R}\ \overline{R}'}{\overline{R} + \overline{R}'} \qquad \ldots(6.19)$$

From this it can be seen that if the input and output coupling are identical and $Z_o = Z_o'$, then $\overline{R}' = 1$ and therefore $\overline{R}' \,//\, \overline{R}$ is always less than 1 which means the cavity is undercoupled.

In the case of the two port cavity, R_{eg}, C_{eg} and L_{eg} can be found from Q_o and Q_1 measurements using the relations given by Altman (17),

$$\overline{R} = \frac{Q_o}{Q_{e_1}} \qquad \ldots(6.20)$$

$$\overline{R}' = \frac{Q_{e_2}}{Q_{e_1}} \qquad \ldots(6.21)$$

$$Q_o = \overline{C}\ \overline{R}\ \omega_o \qquad \ldots(6.22)$$

$$\omega_o = \frac{1}{\sqrt{\overline{L}\ \overline{C}}} \qquad \ldots(6.23)$$

and the expression (5.2),

$$\frac{1}{Q_1} = \frac{1}{Q_o} + \frac{1}{Q_{e_1}} + \frac{1}{Q_{e_2}}$$

For identical input and output coupling,

$$Q_{e_1} = Q_{e_2} = Q_e$$

and with substitution of the expression (6.20), (5.2) becomes:

$$\frac{1}{Q_l} = \frac{1}{Q_o} + \frac{2\overline{R}}{Q_o} \qquad \ldots(6.24)$$

Therefore,

$$\overline{R} = \frac{1}{2}\left(\frac{Q_o}{Q_l} - 1\right) \qquad \ldots(6.25)$$

and $\overline{R'} = 1$

6.4 GAP CAPACITANCE MEASUREMENTS OF THE CAPACITIVE COUPLED TRIANGULAR RESONATOR

A common coupling structure for microstrip is the gap coupling. An equal input and output coupling coefficient for symmetrical structure like a disk or rectangle, can be realized by two identical gaps. In the case of the triangular resonator, in order to have equal coupling coefficients, the input and output gaps should be different. For the latter structure, the relation between the gap width and the capacitance is shown in Fig. 6.4 . This graph was plotted by measuring the gap capacitance of a x10 model triangular resonator on a HP 4270A automatic

capacitance bridge. As a comparison, the capacitance of gaps in a 50 Ω transmission lines is also plotted. The later graph was published in the Microwave Engineers Handbook and Buyer's Guide 1969.

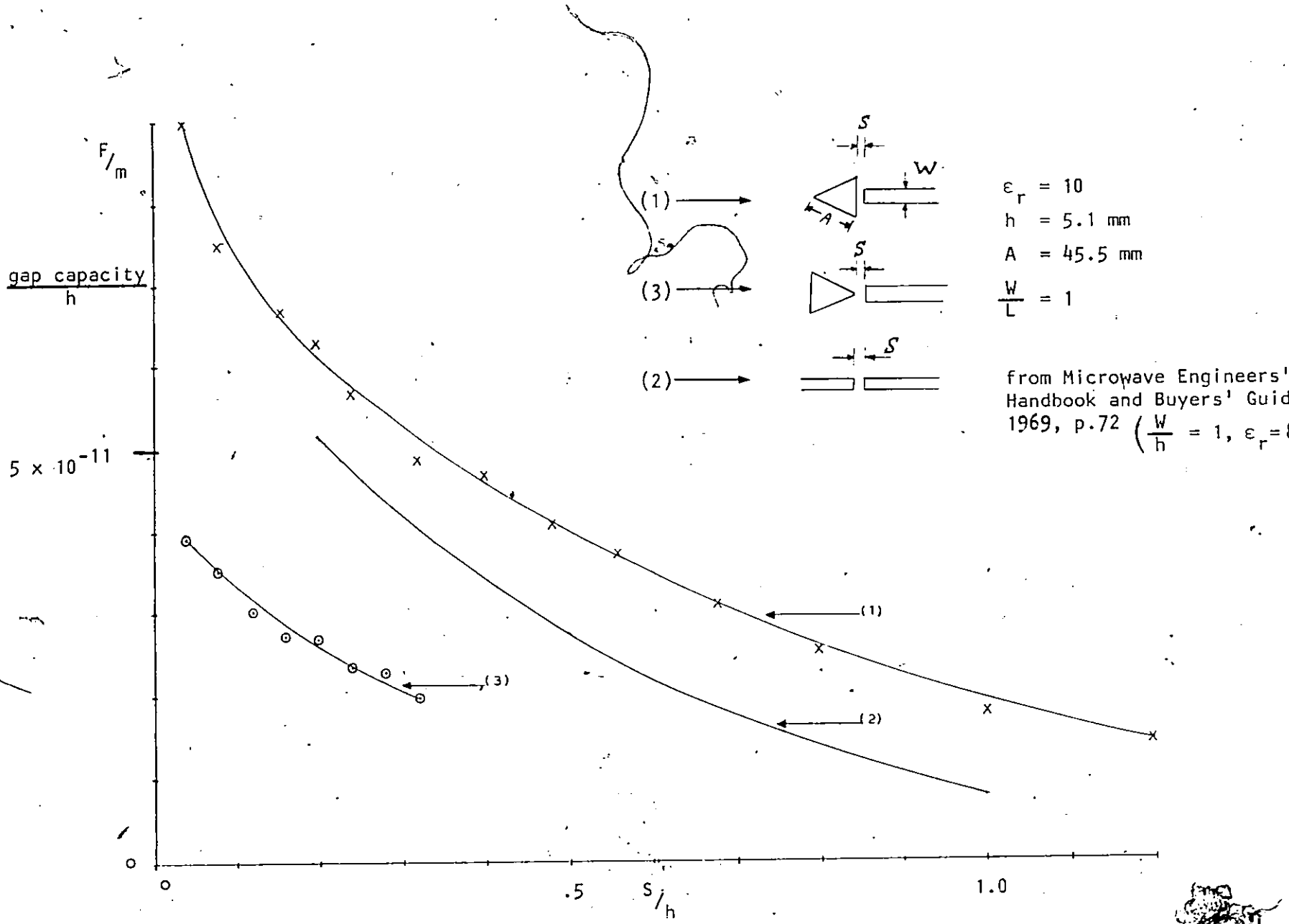

Fig. 6.4 - (Gap Capacitance/substrate thickness) versus (Gap width/substrate thickness)

CHAPTER VII

CONCLUSION

The objective of the thesis was to derive an expression for the radiation loss from triangular microstrip resonators and to verify the theoretical results by measurements. Theoretical results for the radiated power were obtained by numerically integrating the electric far field of the resonator.

The measurement of the radiated power was made in an anechoic chamber. The measured radiation pattern followed qualitatively the theoretically predicted pattern. Since the theoretical derivation contained an arbitrary amplitude factor, $A_{1,0,-1}$ an absolute comparison with the measured results could not be made. The radiation loss measurements overcame the above problem. The theoretical results proved to be in good agreement with measurements for substrates with low dielectric constant, but for high dielectric constant values they differed by a factor of about two as shown in Fig. 7.1 and Fig. 7.2. This discrepancy could be due to the two assumptions made about the dielectric media viz.

i) the permittivity, ε, in section 2.4 was assumed independent of the 'z' direction and taken to be equal to the effective permittivity, ε_e.

ii) ε_e, which is a function of 'x' according to the expression (3.12), was assumed constant.

The results show that for large values of ε_r, the theory underestimates the radiation losses.

Resonators in general have wide circuit applications, but the triangular structure with its 120° symmetry is particularly suited to the fabrication of 3 port ferrite circulators. The experimental comparison between circular and triangular resonators showed that the triangular configuration radiates the least Fig. 5.3. Although the difference is small, it provides useful information for the design of a low loss microstrip circulator. For filters, the rectangular resonator, which is nothing but a resonant section of transmission line, is the simplest structure to use. It also radiates less than the circular or triangular resonators [5,7,8,9]. The radiation pattern of triangular resonators show a large beamwidth, which is one of the characteristics of microstrip structures [16]. The measured E-plane and H-plane 3dB beamwidth is respectively 180° and 100°. However, a more directional antenna can be designed with an array of single elements [14]. The present study also shows that the circular resonator is a better candidate for antenna elements since it radiates more than the triangular one.

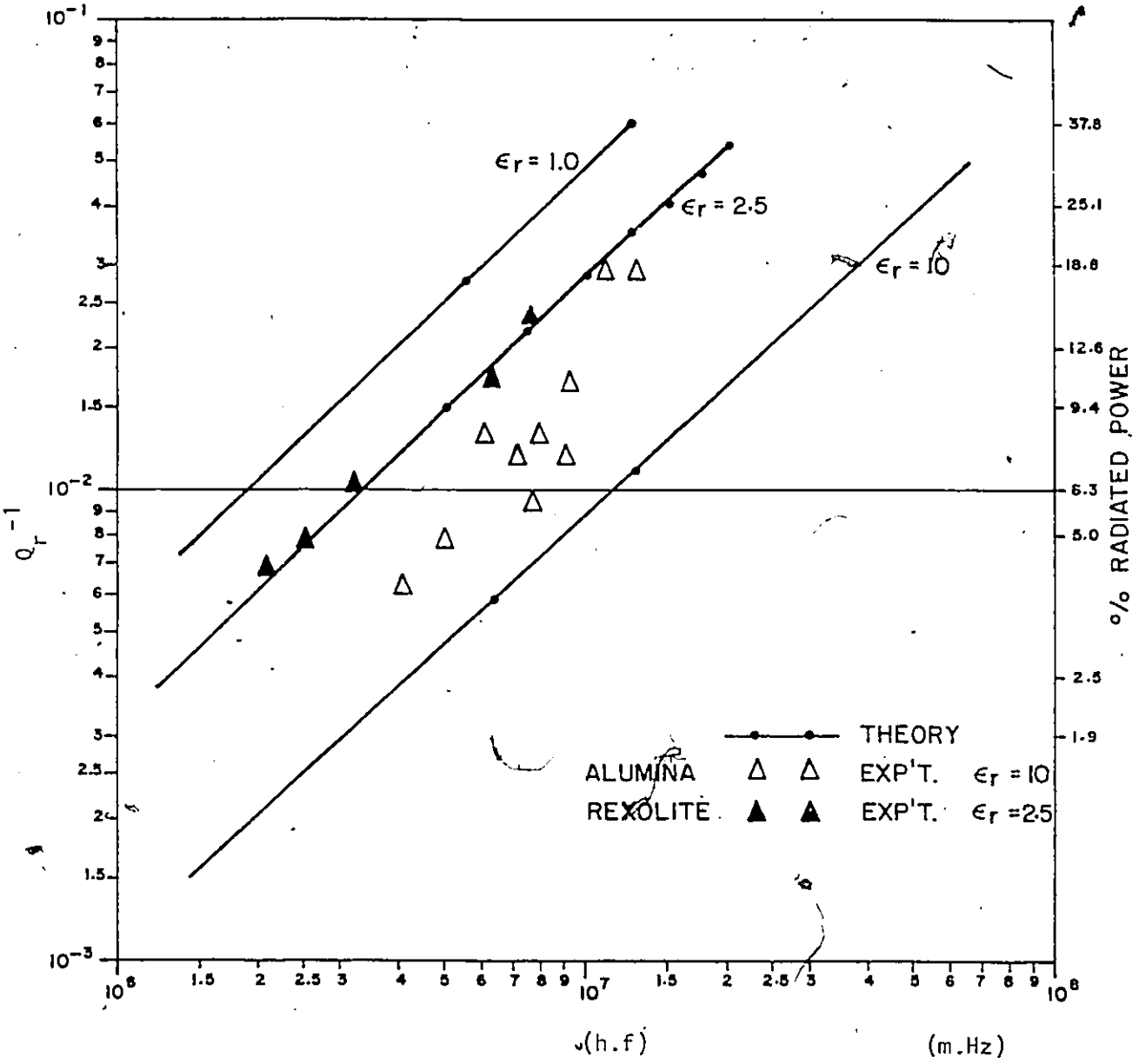

Fig. 7.1 - Experimental and computed values of Q_r^{-1} versus (h.f)

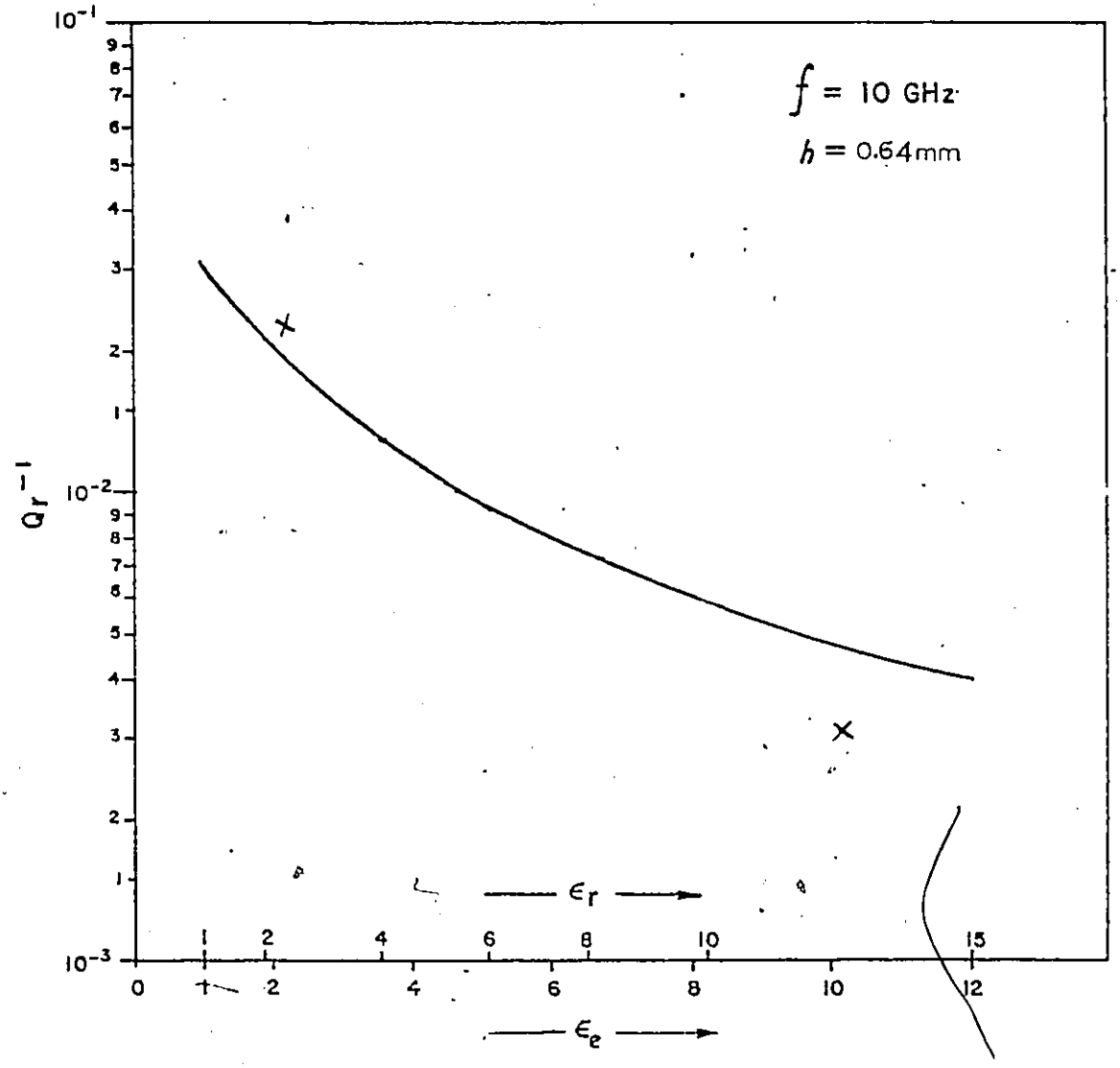

Fig. 7.2 - Experimental and computed values of Q_r^{-1} versus (ε_e) and (ε_r)

——— computed curve

x experimental points

APPENDIX A

1. THE COORDINATE SYSTEM

The coordinate system for the triangular resonator is defined as in Fig. A.1 .

A point P in space can be described as:

$$x_o = r_o \sin\theta \cos\phi \qquad \ldots A.1$$

$$y_o = r_o \sin\theta \cos\phi \qquad \ldots A.2$$

$$z_o = r_o \cos\theta \qquad \ldots A.3$$

2. APPROXIMATE EXPRESSION FOR THE DISTANCE r:

From Fig. A.1 , the distance between the field point P and any point M on the triangle is:

$$r = \sqrt{(x_o - x)^2 + (y_o - y)^2 + (z_o - z)^2} \qquad \ldots A.4$$

Using the far-field considerations, $x_o >> x$, $y_o >> y$, $z_o >> z$, we can neglect the second order terms in x, y, z.

$$r \cong \sqrt{x_o^2 + y_o^2 + z_o^2 - 2(x_o x + y_o y + z_o z)} \qquad \ldots A.5$$

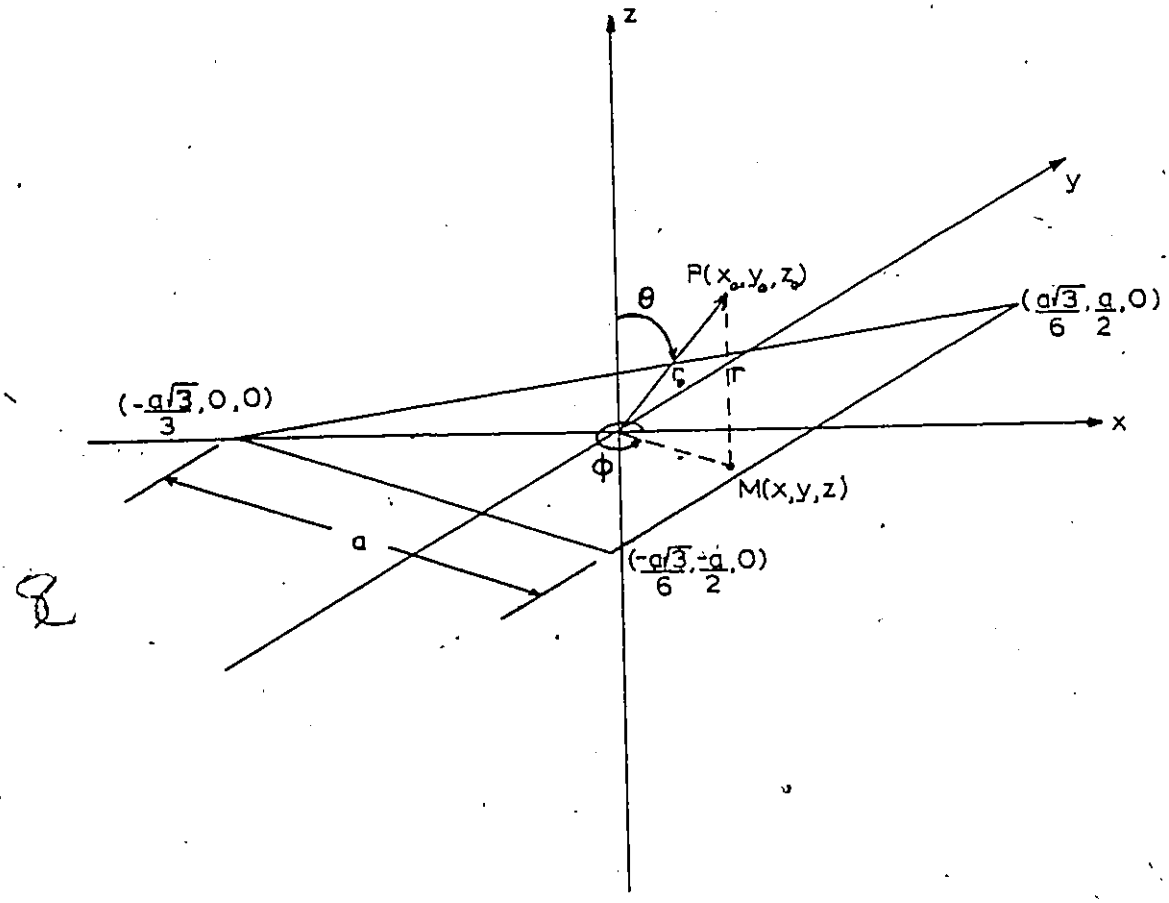

Fig. A.1 - Rectangular and circular coordinate system used in the theoretical analysis

The above expression can be simplified to:

$$r = r_o - \frac{x_o}{r_o} x - \frac{y_o}{r_o} y - \frac{z_o}{r_o} z \qquad \ldots A.6$$

using the binomial expansion and neglecting the higher order terms.

3. TRANSFORMATION FROM CARTESIAN TO SPHERICAL COORDINATES

This transformation can be achieved through multiplying the cartesian coordinate system matrix by the transformation matrix $[T]$.

$$[T] = \begin{bmatrix} \sin\theta\cos\phi & \sin\theta\sin\phi & -\cos\theta \\ \cos\theta\cos\phi & \cos\theta\sin\phi & -\sin\theta \\ -\sin\phi & \cos\phi & 0 \end{bmatrix} \qquad \ldots A.7$$

The spherical coordinate system components in terms of the rectangular components are expressed as:

$$\left.\begin{aligned} C_r &= C_x \sin\theta\cos\phi + C_y \sin\theta\sin\phi + C_z \cos\theta \\ C_\theta &= C_x \cos\theta\cos\phi + C_y \cos\theta\sin\phi - C_z \sin\theta \\ C_\phi &= -C_x \sin\phi + C_y \cos\phi \end{aligned}\right\} \qquad \ldots A.8$$

4. CHANGE OF VARIABLES

The following change of variables is used in Appendix B to simplify calculations.

Let,
$$\alpha = \frac{2\pi}{\sqrt{3}\,a} x + \frac{2\pi}{3} \qquad \ldots A.9$$

And $$\beta = \frac{2\pi}{3a} y \qquad \ldots A.10$$

Thus $$x = -\frac{a\sqrt{3}}{3} \text{ corresponds to } \alpha = 0 \qquad \ldots A.11$$

$$x = \frac{a\sqrt{3}}{6} \text{ corresponds to } \alpha = \pi \qquad \ldots A.12$$

$$y = -\left(\frac{x}{\sqrt{3}} + \frac{a}{3}\right) \text{ corresponds to } \beta = \frac{-\alpha}{3} \qquad \ldots A.13$$

$$y = \left(\frac{x}{\sqrt{3}} + \frac{a}{3}\right) \text{ corresponds to } \beta = \frac{\alpha}{3} \qquad \ldots A.14$$

Also $$y = \frac{3a}{2\pi}\beta \,, \quad x = \frac{\sqrt{3}a}{2\pi}\alpha - 3 \qquad \ldots A.15$$

$$dy = \frac{3a}{2\pi} d\beta \,, \quad dx = \frac{\sqrt{3}a}{2\pi} d\alpha \qquad \ldots A.16$$

APPENDIX B

DERIVATION OF THE HERTZ VECTOR FOR THE TRIANGULAR RESONATOR

In section 3.2, the hertzian vector was simplified to:

$$\vec{\Pi} = -j \frac{30}{k} \frac{e^{-jkr_o}}{r_o} \int_{\tau} e^{jk\left(\frac{x_o}{r_o}x + \frac{y_o}{r_o}y + \frac{z_o}{r_o}z\right)} \vec{J}\, d\tau$$

The expression for the current density was:

$$\vec{J} = \vec{J}_T = \left\{ - H_y(x,y,h) + H_y(x,y,-h) \right\} \vec{a}_x + \left\{ H_x(x,y,h) - H_x(x,y,-h) \right\} \vec{a}_y + \left\{ j\frac{k}{120\pi} \left(\epsilon_e - 1\right) E_z(x,y,0) \right\} \vec{a}_z$$

The above integration is carried out separately for each component of the vector $\vec{\Pi}$. The limits of integration in the x and y directions are defined in Appendix A, Fig. A.1. The integration in the z direction is carried out first and is evaluated at z = h and z = -h since the fields are assumed constant in the z direction.

$$\Pi_x = -j\frac{30}{k}\frac{e}{r_o}^{-jkr_o}\iiint e^{jk\left(\frac{x_o}{r_o}x + \frac{y_o}{r_o}y + \frac{z_o}{r_o}z\right)}\left\{-H_y(x,y,h) + H_y(x,y,-h)\right\}dzdydx$$

$$\Pi_x = -j\frac{30}{k}\frac{e}{r_o}^{-jkr_o}\left\{-e^{j\frac{kz_oh}{r_o}}\iint e^{jk\left(\frac{x_o}{r_o}x + \frac{y_o}{r_o}y\right)}\ H_y(x,y,h)\ dydx\right.$$

$$\left. + e^{-j\frac{kz_oh}{r_o}}\iint e^{jk\left(\frac{x_o}{r_o}x + \frac{y_o}{r_o}y\right)}\ H_y(x,y,-h)\ dydx\right\}$$

as $H_y(x,y,h) = H_y(x,y,-h)$,

$$\Pi_x = -j\frac{30}{k}\frac{e}{r_o}^{-jkr_o}\left\{-2j\left(\frac{e^{j\frac{kz_oh}{r_o}} - e^{-j\frac{kz_oh}{r_o}}}{2j}\right)\right.$$

$$\left.\iint e^{jk\left(\frac{x_o}{r_o}x + \frac{y_o}{r_o}y\right)}\ H_y\ (x,y,h)\ dydx\right\}$$

$$\Pi_x = -\frac{60}{k}\frac{e}{r_o}^{-jkr_o}\ \sin\left(\frac{kz_oh}{r_o}\right)\iint e^{jk\left(\frac{x_o}{r_o}x + \frac{y_o}{r_o}y\right)}\ H_y(x,y,h)\ dydx$$

Using the same approach for Π_y and Π_z

$$\Pi_y = \frac{60}{k}\frac{e}{r_o}^{-jkr_o}\sin\left(\frac{kz_oh}{r_o}\right)\iint e^{jk\left(\frac{x_o}{r_o}x + \frac{y_o}{r_o}y\right)}\ H_x(x,y,h)\ dydx$$

$$\Pi_z = 30\frac{e}{r_o}^{-jkr_o}\frac{(\varepsilon_e - 1)}{120\ \pi}\left[\frac{2r_o}{kz_o}\ \sin\left(\frac{kz_oh}{r_o}\right)\right]\iint e^{jk\left(\frac{x_o}{r_o}x + \frac{y_o}{r_o}y\right)}\ E_z(x,y,0)dydx$$

The limits of integration are:

$$-\frac{a\sqrt{3}}{3} \leq x \leq \frac{a\sqrt{3}}{6} \quad \text{and} \quad -\left(\frac{x}{\sqrt{3}} + \frac{a}{3}\right) \leq y \leq \left(\frac{x}{\sqrt{3}} + \frac{a}{3}\right)$$

The above integrations are carried out after performing the change of variables described in Appendix A.

The x component of the vector Π becomes:

$$\Pi_x = -\frac{60}{k}\frac{e^{-jkr_o}}{r_o}\sin\left(\frac{kz_o h}{r_o}\right)\int_o^{\pi}\int_{\frac{-\alpha}{3}}^{\frac{\alpha}{3}} e^{j\frac{kx_o}{r_o}\left\{\frac{\sqrt{3}a}{2\pi}\alpha - 3\right\}} e^{j\frac{ky_o}{r_o}\frac{3a}{2\pi}\beta}$$

$$\left\{j\sqrt{3}\, A_{1,0,-1}\ \xi_e\ (\sin\alpha\cos\beta)\right\}\ \frac{3\sqrt{3}a^2}{4\pi^2}\, d\beta d\alpha$$

Let $C_x = -j\frac{60}{k}\xi_e A_{1,0,-1}\left(\frac{3a}{2\pi}\right)^2 \sin\left(\frac{kz_o h}{r_o}\right)\frac{e^{-jk\left(r_o + \frac{3x_o}{r_o}\right)}}{r_o}$

$$m = \frac{3kx_o}{r_o}\frac{\sqrt{3}a}{2\pi} \qquad n = \frac{ky_o}{r_o}\frac{3a}{2\pi}$$

Then,

$$\Pi_x = C_x \int_o^{\pi}\int_{\frac{-\alpha}{3}}^{\frac{\alpha}{3}} e^{j\frac{m\alpha}{3}}\ e^{jn\beta}\ (\sin\alpha\cos\beta)\ d\alpha d\beta$$

From integral tables we have,

$$\int e^{a\gamma}\cos b\gamma d\gamma = \frac{e^{a\gamma}}{b^2 + a^2}\left(a\cos b\gamma + b\sin b\gamma\right)$$

Therefore,

$$\Pi_x = C_x \int_0^{\pi} \left(e^{j\frac{m\alpha}{3}} \sin\alpha \right) \left[\frac{e^{jn\beta}}{1 - n^2} \left(jn\cos\beta + \sin\beta \right) \right]_{-\frac{\alpha}{3}}^{\frac{\alpha}{3}} d\alpha$$

$$\Pi_x = C_x \int_0^{\pi} \left(e^{j\frac{m\alpha}{3}} \sin\alpha \right) \left[\frac{jn\cos\frac{\alpha}{3}}{1 - n^2} \left(e^{j\frac{n\alpha}{3}} - e^{-j\frac{n\alpha}{3}} \right) + \frac{\sin\frac{\alpha}{3}}{1 - n^2} \left(e^{j\frac{n\alpha}{3}} + e^{-j\frac{n\alpha}{3}} \right) \right] d\alpha$$

The above expression can be rearranged to:

$$\Pi_x = \frac{C_x}{4(1 - n^2)} \int_0^{\pi} \left[(n - 1) e^{j\frac{\alpha}{3}} P_1 + (n + 1) e^{j\frac{\alpha}{3}} P_2 - (n + 1) e^{j\frac{\alpha}{3}} P_3 \right.$$

$$- (n - 1) e^{j\frac{\alpha}{3}} P_4 - (n - 1) e^{j\frac{\alpha}{3}} P_5 - (n + 1) e^{j\frac{\alpha}{3}} P_6$$

$$\left. + (n + 1) e^{j\frac{\alpha}{3}} P_7 + (n - 1) e^{j\frac{\alpha}{3}} P_8 \right] d\alpha$$

with $P_1 = m + n + 4$, $P_2 = m + n + 2$, $P_3 = m - n + 4$

$P_4 = m - n + 2$, $P_5 = m + n - 2$, $P_6 = m + n - 4$

$P_7 = m - n - 2$, $P_8 = m - n - 4$

The result of the second integration is:

$$\Pi_x = j\,\frac{3\,C_x}{4(1-n^2)}\left[\frac{(n-1)}{P_1}\left(e^{j\frac{\pi}{3}P_1}-1\right)+\frac{(n+1)}{P_2}\left(e^{j\frac{\pi}{3}P_2}-1\right)\right.$$
$$-\frac{(n+1)}{P_3}\left(e^{j\frac{\pi}{3}P_3}-1\right)-\frac{(n-1)}{P_4}\left(e^{j\frac{\pi}{3}P_4}-1\right)$$
$$-\frac{(n-1)}{P_5}\left(e^{j\frac{\pi}{3}P_5}-1\right)-\frac{(n+1)}{P_6}\left(e^{j\frac{\pi}{3}P_6}-1\right)$$
$$\left.+\frac{(n+1)}{P_7}\left(e^{j\frac{\pi}{3}P_7}-1\right)+\frac{(n-1)}{P_8}\left(e^{j\frac{\pi}{3}P_8}-1\right)\right]$$

Using the same approach Π_y and Π_z is found to be:

$$\Pi_y = \frac{3\,C_y}{4(1-n^2)}\left[\frac{(n-1)}{P_1}\left(e^{j\frac{\pi}{3}P_1}-1\right)+\frac{(n+1)}{P_2}\left(e^{j\frac{\pi}{3}P_2}-1\right)\right.$$
$$-\frac{(n+1)}{P_3}\left(e^{j\frac{\pi}{3}P_3}-1\right)-\frac{(n-1)}{P_4}\left(e^{j\frac{\pi}{3}P_4}-1\right)$$
$$+\frac{(n-1)}{P_5}\left(e^{j\frac{\pi}{3}P_5}-1\right)+\frac{(n+1)}{P_6}\left(e^{j\frac{\pi}{3}P_6}-1\right)$$
$$\left.-\frac{(n+1)}{P_7}\left(e^{j\frac{\pi}{3}P_7}-1\right)-\frac{(n-1)}{P_8}\left(e^{j\frac{\pi}{3}P_8}-1\right)\right]$$

$$-j\frac{3\,C_y}{2(4-n^2)}\left[\frac{(n-2)}{P_2}\left(e^{j\frac{\pi}{3}P_2}-1\right)+\frac{(n+2)}{P_4}\left(e^{j\frac{\pi}{3}P_4}-1\right)\right.$$
$$\left.+\frac{(n+2)}{P_5}\left(e^{j\frac{\pi}{3}P_5}-1\right)-\frac{(n-2)}{P_7}\left(e^{j\frac{\pi}{3}P_7}-1\right)\right]$$

where $C_y = C_x/\sqrt{3}$

$$\Pi_z = \frac{3\,C_z}{2(1-n^2)}\left[\frac{(n-1)}{P_1}\left(e^{j\frac{\pi}{3}P_1}-1\right)+\frac{(n+1)}{P_2}\left(e^{j\frac{\pi}{3}P_2}-1\right)\right.$$

$$-\frac{(n+1)}{P_3}\left(e^{j\frac{\pi}{3}P_3}-1\right)-\frac{(n-1)}{P_4}\left(e^{j\frac{\pi}{3}P_4}-1\right)$$

$$+\frac{(n-1)}{P_5}\left(e^{j\frac{\pi}{3}P_5}-1\right)+\frac{(n+1)}{P_6}\left(e^{j\frac{\pi}{3}P_6}-1\right)$$

$$\left.-\frac{(n+1)}{P_7}\left(e^{j\frac{\pi}{3}P_7}-1\right)-\frac{(n-1)}{P_8}\left(e^{j\frac{\pi}{3}P_8}-1\right)\right]$$

$$+\frac{3\,C_z}{2(4-n^2)}\left[\frac{(n-2)}{P_2}\left(e^{j\frac{\pi}{3}P_2}-1\right)-\frac{(n+2)}{P_4}\left(e^{j\frac{\pi}{3}P_4}-1\right)\right.$$

$$\left.+\frac{(n+2)}{P_5}\left(e^{j\frac{\pi}{3}P_5}-1\right)-\frac{(n-2)}{P_7}\left(e^{j\frac{\pi}{3}P_7}-1\right)\right]$$

where

$$C_z = \frac{30(\varepsilon_e-1)}{120\pi\sqrt{3}}\left\{\frac{2r_o}{kz_o}\sin\left(\frac{kz_o h}{r_o}\right)\right\}\left(\frac{3a}{2\pi}\right)^2 e^{-jk\left(r_o+\frac{3x_o}{r_o}\right)} A_{1,0,-1}$$

APPENDIX C

COMPUTER PROGRAM TO CALCULATE THE RADIATION LOSS OF A TRIANGULAR RESONATOR

The input to the program consists of the length of the triangle's side (mm), the substrate thickness (mm) and the relative dielectric constant. The print-out contains the resonance frequency (Hz), the effective dielectric constant, the radiated power (W), the stored energy times the frequency (ω), the percentage radiated power, the radiation Q and the product h . f (m.Hz). The program uses a computer library subroutine to calculate a double integration.

```
C     ******** THIS PROGRAM CALCULATES THE POWER RADIATED
C     FROM A TRIANGULAR SHAPED MICROSTRIP RESONATOR ********
C
C
C     THIS IS THE MAIN PROG.
      EXTERNAL F,INTPOW,FY1,FY2
      COMMON A,H,EPSREL,EPSEFF,R0,A101,PI,CX,CY,CZ
      IMPLICIT DOUBLE PRECISION (A-Z)
      INTEGER YES
      WRITE(108,80)
 80   FORMAT(///,2X,'RADIATION ANALYSIS OF THE TRIANGULAR RESONATOR')
 100    WRITE(108,5)
 5    FORMAT(/,' ENTER TRIANGLE SIDE LENGTH IN MM ,SUBSTRATE THICKNESS
      WRITE(108,51)
 51   FORMAT(' IN MM ,RELATIVE  DIELECTRIC CONST. ')
      WRITE(108,52)
 52   FORMAT(' ALL NUMBERS IN  * G* FORM ')
      READ(105,1)  A,H,EPSREL
 1    FORMAT(3G)
      PI=3.1415926535D0
      A=1.D-3*A
      H=1.D-3*H
      A101=1.D0
      R0=1.D0
      W=(A*DSQRT(3.D0))/3.D0
      HOVERW=1.D0+((10.D0*H)/W)
      EPSEFF=((EPSREL+1.D0)/2.D0)+(((EPSREL-1.D0)/2.D0)
     1*(1.D0/DSQRT(HOVERW)))
      EPS=1.D-9/(PI*36.D0)
      STENE=(EPSREL*EPS*H*(A**2)*9.D0*(DSQRT(3.D0)))/48.D0
      RFREQ=2.D8/(A*DSQRT(EPSREL))
      STPOW=STENE*RFREQ
      WRITE(108,9)
 9    FORMAT(////,' THE RESONANCE FREQUENCY IN HZ. IS')
      WRITE(108,8) RFREQ
 8    FORMAT(2X,D16.8)
      WRITE(108,46)
 46   FORMAT(2X,' THE EFFECTIVE DIELECTRIC CONSTANT IS    ')
      WRITE(108,47) EPSEFF
 47   FORMAT(2X,D16.8,/)
      CALL DBLEINTG(DINTG,0.0,1.5707963267,FY1,FY2,
     1.1,F,INTPOW)
C
C     THE INTEGRATION LIMITS ARE  THETA=0 TO PI/2
C     PHI=0 TO 2*PI
C
      ANSWER=DINTG/(2.D0*120.D0*PI)
      CORQR=((2.D0*PI*RFREQ*STENE)-ANSWER)/ANSWER
      PERAD=(ANSWER*100.D0)/STPOW
      WRITE(108,20)
```

```
51.000   20    FORMAT('------  THE RADIATED POWER IS -------- ')
52.000         WRITE(108,21) ANSWER
53.000   21    FORMAT(30X,D16.8)
54.000         WRITE(108,60)
55.000   60    FORMAT(' ------ STORED ENERGY * 'F' --------')
56.000         WRITE(108,21) STPOW
57.000         WRITE(108,70)
58.000   70    FORMAT(2X,'______PERCENTAGE RADIATED POWER ______')
59.000         WRITE(108,71) PPRAD
60.000   71    FORMAT(30X,D16.8)
61.000         QQRAD=(2.D0*PI*100.D0)/PPRAD
62.000         WRITE(108,72)
63.000   72    FORMAT(2X,'_____RADIATION Q _____')
64.000         WRITE(108,71) QQRAD
65.000         HF=H*RFREQ
66.000         WRITE(108,61)
67.000   61    FORMAT('-----CORRECTED RADIATION Q -----')
68.000         WRITE(108,71) CORQR
69.000         WRITE(108,41)
70.000   41    FORMAT('----------  d*F ----------')
71.000         WRITE(108,71) HF
72.000         WRITE(108,22)
73.000   22    FORMAT(//,' IF YOU WANT TO CONTINUE ENTER 1/IF NOT ENTER 0 :)
74.000         READ(108,24) YES
75.000   24    FORMAT(1G)
76.000         IF (YES.EQ.1.) GO TO 100
77.000         STOP
78.000         END
79.000 C
80.000 C       SECOND INTEGRAL LOWER LIMIT
81.000 C       PHI=0
82.000 C
83.000         FUNCTION FY1(XXXX)
84.000         IMPLICIT DOUBLE PRECISION(A-Z)
85.000         FY1=0.D0
86.000         RETURN
87.000         END
88.000 C
89.000 C       SECOND INTEGRAL UPPER LIMIT
90.000 C       PHI=2*3.1416
91.000 C
92.000         FUNCTION FY2(XXXX)
93.000         IMPLICIT DOUBLE PRECISION(A-Z)
94.000         FY2=3.14159265400*2.00
95.000         RETURN
96.000         END
97.000 C
98.000 C
99.000 C       THIS IS THE FUNCTION SUB TO CALCULATE THE INTEGRAL FCN.
100.000 C
```

```
101.000 C
102.000       FUNCTION INTPOW(THETA,PHI)
103.000       IMPLICIT DOUBLE PRECISION(A-Z)
104.000       DOUBLE COMPLEX ZZ,ZX1,ZX2,ZX3,ZX4,ZX5,ZX6,ZX7,ZX8,ZXX,
105.000      1PIX,ZYY,PIY,ZZZ,PIZ,ETHETA,EPHI
106.000       COMMON A,H,EPSREL,EPSEFF,R0,A101,PI,CX,CY,CZ
107.000       YOR0=DSIN(THETA)*DCOS(PHI)
108.000       XOR0=DSIN(THETA)*DSIN(PHI)
109.000       ZOR0=DCOS(THETA)
110.000       K=4.D0*PI/(3.D0*A*DSQRT(EPSREL))
111.000       GAMMA=K*ZOR0*H
112.000       M=(3.D0*K*XOR0*A*DSQRT(3.D0))/(2.D0*PI)
113.000       N=3.D0*K*YOR0*A/(2.D0*PI)
114.000       PSI1=DSQRT(EPSREL)/(1.2D2*PI)
115.000       PSI2=1.D0/(1.2D2*PI)
116.000       GAMMA1=M+N+2.D0
117.000       GAMMA2=M+N-2.D0
118.000       GAMMA3=M-N+2.D0
119.000       GAMMA4=M-N-2.D0
120.000       OMEGA1=M+N+4.D0
121.000       OMEGA2=M+N-2.D0
122.000       OMEGA3=M+N+2.D0
123.000       OMEGA4=M+N-4.D0
124.000       OMEGA5=M-N+4.D0
125.000       OMEGA6=M-N-2.D0
126.000       OMEGA7=M-N+2.D0
127.000       OMEGA8=M-N-4.D0
128.000       B1=N-1.D0
129.000       B2=N+1.D0
130.000       B3=N-2.D0
131.000       B4=N+2.D0
132.000       D=K*R0+3.D0*XOR0*K
133.000       CY=(3.D1*A101*PSI1*((3.D0*A)**2)*DSIN(GAMMA))/(DSQRT(3.D0)
134.000      1*K*R0*((2.D0*PI)**2))
135.000       CX=CY*DSQRT(3.D0)
136.000       CZ=(3.D1*PSI2*(EPSEFF-1.D0)*A101*2.D0*((3.D0*A)**2)*
137.000      1DSIN(GAMMA))/(DSQRT(3.D0)*((2.D0*PI)**2)*ZOR0*K*R0)
138.000       L2=3.D0/(2.D0*(1-N**2))
139.000       L1=3.D0/(4.D0-N**2)
140.000       QY1=L1*B3/GAMMA1
141.000       QY2=L1*B4/GAMMA2
142.000       QY3=L1*B4/GAMMA3
143.000       QY4=L1*B3/GAMMA4
144.000       TY1=L2*B1/OMEGA1
145.000       TY2=L2*B1/OMEGA2
146.000       TY3=L2*B2/OMEGA3
147.000       TY4=L2*B2/OMEGA4
148.000       TY5=L2*B2/OMEGA5
149.000       TY6=L2*B2/OMEGA6
150.000       TY7=L2*B1/OMEGA7
```

```
151.000       TY8=L2*R1/OMEGA8
152.000       ZZ=DCMPLX(0.D0,-D)
153.000       AYSEL=TY1*DCOS(OMEGA1*PI/3.D0)-TY1-TY2*DCOS(OMEGA2*PI/3.D0)
154.000      1+TY2+TY3*DCOS(OMEGA3*PI/3.D0)-TY3-TY4*DCOS(OMEGA4*PI/3.D0)
155.000      2+TY4-TY5*DCOS(OMEGA5*PI/3.D0)+TY5+TY6*DCOS(OMEGA6*PI/3.D0)
156.000      3-TY6-TY7*DCOS(OMEGA7*PI/3.D0)+TY7+TY8*DCOS(OMEGA8*PI/3.D0)
157.000      4-TY8
158.000       AJDA=TY1*DSIN(OMEGA1*PI/3.D0)-TY2*DSIN(OMEGA2*PI/3.D0)
159.000      1+TY3*DSIN(OMEGA3*PI/3.D0)-TY4*DSIN(OMEGA4*PI/3.D0)
160.000      2-TY5*DSIN(OMEGA5*PI/3.D0)+TY6*DSIN(OMEGA6*PI/3.D0)
161.000      3-TY7*DSIN(OMEGA7*PI/3.D0)+TY8*DSIN(OMEGA8*PI/3.D0)
162.000       ZXX=DCMPLX(AYSEL,AJDA)
163.000       PIX=CX*CDEXP(ZZ)*ZXX
164.000       AYSE=QY1*DCOS(GAMMA1*PI/3.D0)-QY1-QY2*DCOS(GAMMA2*PI/3.D0)
165.000      1+QY2+QY3*DCOS(GAMMA3*PI/3.D0)-QY3-QY4*DCOS(GAMMA4*PI/3.D0)
166.000      2+QY4+TY1*DSIN(OMEGA1*PI/3.D0)+TY2*DSIN(OMEGA2*PI/3.D0)+
167.000      3TY3*DSIN(OMEGA3*PI/3.D0)+TY4*DSIN(OMEGA4*PI/3.D0)-TY5*
168.000      4DSIN(OMEGA5*PI/3.D0)-TY6*DSIN(OMEGA6*PI/3.D0)-TY7*
169.000      5DSIN(OMEGA7*PI/3.D0)-TY8*DSIN(OMEGA8*PI/3.D0)
170.000       FATOS=QY1*DSIN(GAMMA1*PI/3.D0)-QY2*DSIN(GAMMA2*PI/3.D0)+
171.000      1QY3*DSIN(GAMMA3*PI/3.D0)-QY4*DSIN(GAMMA4*PI/3.D0)-
172.000      2TY1*DCOS(OMEGA1*PI/3.D0)-TY2*DCOS(OMEGA2*PI/3.D0)+TY2
173.000      3+TY1-TY3*DCOS(OMEGA3*PI/3.D0)+TY3-TY4*DCOS(OMEGA4*PI/3.D0)
174.000      4+TY4+TY5*DCOS(OMEGA5*PI/3.D0)-TY5+TY6*DCOS(OMEGA6*PI/3.D0)
175.000      5-TY6+TY7*DCOS(OMEGA7*PI/3.D0)-TY7+TY8*DCOS(OMEGA8*PI/3.D0)
176.000      6-TY8
177.000       ZYY=DCMPLX(AYSE,FATOS)
178.000       PIY=CY*CDEXP(ZZ)*ZYY
179.000       FATMA=TY1*DCOS(OMEGA1*PI/3.D0)-TY1+TY2*DCOS(OMEGA2*PI/3.D0)
180.000      1-TY2+TY3*DCOS(OMEGA3*PI/3.D0)-TY3+TY4*DCOS(OMEGA4*PI/3.D0)
181.000      2-TY4-TY5*DCOS(OMEGA5*PI/3.D0)+TY5-TY6*DCOS(OMEGA6*PI/3.D0)
182.000      3+TY6-TY7*DCOS(OMEGA7*PI/3.D0)+TY7-TY8*DCOS(OMEGA8*PI/3.D0)
183.000      4+TY8+(QY1*DCOS(GAMMA1*PI/3.D0)-QY1+QY2*DCOS(GAMMA2*PI/3.D0)
184.000      5-QY2-QY3*DCOS(GAMMA3*PI/3.D0)+QY3-QY4*DCOS(GAMMA4*PI/3.D0)
185.000      6+QY4)*0.5D0
186.000       INCI=TY1*DSIN(OMEGA1*PI/3.D0)+TY2*DSIN(OMEGA2*PI/3.D0)+
187.000      1TY3*DSIN(OMEGA3*PI/3.D0)+TY4*DSIN(OMEGA4*PI/3.D0)-
188.000      2TY5*DSIN(OMEGA5*PI/3.D0)-TY6*DSIN(OMEGA6*PI/3.D0)-
189.000      3TY7*DSIN(OMEGA7*PI/3.D0)-TY8*DSIN(OMEGA8*PI/3.D0)+(
190.000      4QY1*DSIN(GAMMA1*PI/3.D0)+QY2*DSIN(GAMMA2*PI/3.D0)-QY3*
191.000      5DSIN(GAMMA3*PI/3.D0)-QY4*DSIN(GAMMA4*PI/3.D0))*0.5D0
192.000       ZZZ=DCMPLX(FATMA,INCI)
193.000       PIZ=CZ*CDEXP(ZZ)*ZZZ
194.000 C
195.000 C     FAR FIELD  E-VECTOR THETA AND PHI
196.000 C     COMPONANTS
197.000 C
198.000       ETHETA=(K**2)*(PIY*DCOS(THETA)*DSIN(PHI)+PIX*DCOS(THETA)*DCOS(PHI
199.000      1-PIZ*DSIN(THETA))
200.000       EPHI=(K**2)*(PIY*DCOS(PHI)-PIX*DSIN(PHI))
201.000       RADPOW=(CDABS(ETHETA))**2+(CDABS(EPHI))**2
202.000       INTPOW=RADPOW*DSIN(THETA)*(R0**2)
203.000       RETURN
204.000       END
```

APPENDIX D

COMPUTER PROGRAM TO FIND THE RADIATION PATTERN OF A TRIANGULAR RESONATOR

This program requires the starting point (the angles θ and ϕ) in addition to A, h and ε_r. In the program, θ varies from 0 to 90° with increments of 10° while ϕ is held constant. The printed results are θ, the modules of the far-field E vector in the θ direction, the modules of the far-field E vector in the ϕ direction and the poynting vector at that point.

```
1.000 C     THIS IS THE PROGRAM TO CALCULATE THE RADIATION PATTERN
2.000 C     OF A TRIANGULAR RESONATOR.
3.000       IMPLICIT DOUBLE PRECISION(A-Z)
4.000       INTEGER J
5.000       DOUBLE COMPLEX ZZ,ZX1,ZX2,ZX3,ZX4,ZX5,ZX6,ZX7,ZX8,ZXX,
6.000      1PIX,ZYY,PIY,ZZZ,PIZ,ETHETA,EPHI
7.000       WRITE(108,11)
8.000  11   FORMAT('----- ENTER TRIANGLE SIDE LENGTH, SUBSTRATE ')
9.000       WRITE(108,12)
10.000 12   FORMAT(' THICKNESS, IN MILS, RELATIVE DIELEC. CONSTANT--')
11.000      READ(105,13) A,H,EPSREL
12.000 13   FORMAT(3G)
13.000      WRITE(108,14)
14.000 14   FORMAT(' ENTER THETA AND PHI IN DEGREE ')
15.000      READ(105,15) THETA,PHI
16.000 15   FORMAT(2G)
17.000      WRITE(108,20)
18.000 20   FORMAT(/////,'----- PHI -----')
19.000      WRITE(108,21) PHI
20.000 21   FORMAT(G)
21.000      WRITE(108,22)
22.000 22   FORMAT(//,'----- THETA ----- MOD. ETHETA ----- MOD. EPHI
23.000     1----- POY. VECTOR-----')
24.000      A=2.54D-5*A
25.000      H=2.54D-5*H
26.000      W=(A*DSQRT(3.D0))/3.D0
27.000      HOVERW=1.D0+((10.D0*H)/W)
28.000      EPSEFF=((EPSREL+1.D0)/2.D0)+(((EPSREL-1.D0)/2.D0)
29.000     1*(1.D0/DSQRT(HOVERW)))
30.000      R0=4.D0
31.000      A101=1.D0
32.000      PI=3.141592654D0
33.000      K=4.D0*PI/(3.D0*A*DSQRT(EPSREL))
34.000      PSI1=DSQRT(EPSREL)/(1.2D2*PI)
35.000      PSI2=1.D0/(1.2D2*PI)
36.000      DO 100 J=1,10
37.000      THETA=THETA/57.295779D0
38.000      PHI=PHI/57.295779D0
39.000      YOR0=DSIN(THETA)*DCOS(PHI)
40.000      XOR0=DSIN(THETA)*DSIN(PHI)
41.000      ZOR0=DCOS(THETA)
42.000      GAMMA=K*ZOR0*H
43.000      M=(3.D0*K*XOR0*A*DSQRT(3.D0))/(2.D0*PI)
44.000      N=3.D0*K*YOR0*A/(2.D0*PI)
45.000      GAMMA1=M+N+2.D0
46.000      GAMMA2=M+N-2.D0
47.000      GAMMA3=M-N+2.D0
48.000      GAMMA4=M-N-2.D0
49.000      OMEGA1=M+N+4.D0
50.000      OMEGA2=M+N-2.D0
```

```
      OMEGA3=M+N+2.D0
      OMEGA4=M+N-4.D0
      OMEGA5=M-N+4.D0
      OMEGA6=M-N-2.D0
      OMEGA7=M-N+2.D0
      OMEGA8=M-N-4.D0
      B1=N-1.D0
      B2=N+1.D0
      B3=N-2.D0
      B4=N+2.D0
      D=K*R0+3.D0*X0R0*K
      CY=(3.D1*A101*PSI1*((3.D0*A)**2)*DSIN(GAMMA))/(DSQRT(3.D0)
     1*K*R0*((2.D0*PI)**2))
      CX=CY*DSQRT(3.D0)
      CZ=(3.D1*PSI2*(EPSEFF-1.D0)*A101*2.D0*((3.D0*A)**2)*
     1DSIN(GAMMA))/(DSQRT(3.D0)*((2.D0*PI)**2)*ZOR0*K*R0)
      L2=3.D0/(2.D0*(1-N**2))
      L1=3.D0/(4.D0-N**2)
      QY1=L1*B3/GAMMA1
      QY2=L1*B4/GAMMA2
      QY3=L1*B4/GAMMA3
      QY4=L1*B3/GAMMA4
      TY1=L2*B1/OMEGA1
      TY2=L2*B1/OMEGA2
      TY3=L2*B2/OMEGA3
      TY4=L2*B2/OMEGA4
      TY5=L2*B2/OMEGA5
      TY6=L2*B2/OMEGA6
      TY7=L2*B1/OMEGA7
      TY8=L2*B1/OMEGA8
      ZZ=DCMPLX(0.D0,-D)
      AYSEL=TY1*DCOS(OMEGA1*PI/3.D0)-TY1-TY2*DCOS(OMEGA2*PI/3.D0)
     1+TY2+TY3*DCOS(OMEGA3*PI/3.D0)-TY3-TY4*DCOS(OMEGA4*PI/3.D0)
     2+TY4-TY5*DCOS(OMEGA5*PI/3.D0)+TY5+TY6*DCOS(OMEGA6*PI/3.D0)
     3-TY6-TY7*DCOS(OMEGA7*PI/3.D0)+TY7+TY8*DCOS(OMEGA8*PI/3.D0)
     4-TY8
      AJDA=TY1*DSIN(OMEGA1*PI/3.D0)-TY2*DSIN(OMEGA2*PI/3.D0)
     1+TY3*DSIN(OMEGA3*PI/3.D0)-TY4*DSIN(OMEGA4*PI/3.D0)
     2-TY5*DSIN(OMEGA5*PI/3.D0)+TY6*DSIN(OMEGA6*PI/3.D0)
     3-TY7*DSIN(OMEGA7*PI/3.D0)+TY8*DSIN(OMEGA8*PI/3.D0)
      ZXX=DCMPLX(AYSEL,AJDA)
      PIX=CX*CDEXP(ZZ)*ZXX
      AYSE=QY1*DCOS(GAMMA1*PI/3.D0)-QY1-QY2*DCOS(GAMMA2*PI/3.D0)
     1+QY2+QY3*DCOS(GAMMA3*PI/3.D0)-QY3-QY4*DCOS(GAMMA4*PI/3.D0)
     2+QY4+TY1*DSIN(OMEGA1*PI/3.D0)+TY2*DSIN(OMEGA2*PI/3.D0)+
     3TY3*DSIN(OMEGA3*PI/3.D0)+TY4*DSIN(OMEGA4*PI/3.D0)-TY5*
     4DSIN(OMEGA5*PI/3.D0)-TY6*DSIN(OMEGA6*PI/3.D0)-TY7*
     5DSIN(OMEGA7*PI/3.D0)-TY8*DSIN(OMEGA8*PI/3.D0)
      FATOS=QY1*DSIN(GAMMA1*PI/3.D0)-QY2*DSIN(GAMMA2*PI/3.D0)+
     1QY3*DSIN(GAMMA3*PI/3.D0)-QY4*DSIN(GAMMA4*PI/3.D0)-
```

```
101.000      2TY1*DCOS(OMEGA1*PI/3.D0)-TY2*DCOS(OMEGA2*PI/3.D0)+TY2
102.000      3+TY1-TY3*DCOS(OMEGA3*PI/3.D0)+TY3-TY4*DCOS(OMEGA4*PI/3.D0)
103.000      4+TY4+TY5*DCOS(OMEGA5*PI/3.D0)-TY5+TY6*DCOS(OMEGA6*PI/3.D0)
104.000      5-TY6+TY7*DCOS(OMEGA7*PI/3.D0)-TY7+TY8*DCOS(OMEGA8*PI/3.D0)
105.000      6-TY8
106.000       ZYY=DCMPLX(AYSE,FATOS)
107.000       PIY=CY*CDEXP(ZZ)*ZYY
108.000       FATMA=TY1*DCOS(OMEGA1*PI/3.D0)-TY1+TY2*DCOS(OMEGA2*PI/3.D0)
109.000      1-TY2+TY3*DCOS(OMEGA3*PI/3.D0)-TY3+TY4*DCOS(OMEGA4*PI/3.D0)
110.000      2-TY4-TY5*DCOS(OMEGA5*PI/3.D0)+TY5-TY6*DCOS(OMEGA6*PI/3.D0)
111.000      3+TY6-TY7*DCOS(OMEGA7*PI/3.D0)+TY7-TY8*DCOS(OMEGA8*PI/3.D0)
112.000      4+TY8+(QY1*DCOS(GAMMA1*PI/3.D0)-QY1+QY2*DCOS(GAMMA2*PI/3.D0)
113.000      5-QY2-QY3*DCOS(GAMMA3*PI/3.D0)+QY3-QY4*DCOS(GAMMA4*PI/3.D0)
114.000      6+QY4)*0.5D0
115.000       INCI=TY1*DSIN(OMEGA1*PI/3.D0)+TY2*DSIN(OMEGA2*PI/3.D0)+
116.000      1TY3*DSIN(OMEGA3*PI/3.D0)+TY4*DSIN(OMEGA4*PI/3.D0)-
117.000      2TY5*DSIN(OMEGA5*PI/3.D0)-TY6*DSIN(OMEGA6*PI/3.D0)-
118.000      3TY7*DSIN(OMEGA7*PI/3.D0)-TY8*DSIN(OMEGA8*PI/3.D0)+(
119.000      4QY1*DSIN(GAMMA1*PI/3.D0)+QY2*DSIN(GAMMA2*PI/3.D0)-QY3*
120.000      5DSIN(GAMMA3*PI/3.D0)-QY4*DSIN(GAMMA4*PI/3.D0))*0.5D0
121.000       ZZZ=DCMPLX(FATMA,INCI)
122.000       PIZ=CZ*CDEXP(ZZ)*ZZZ
123.000       ETHETA=(K**2)*(PIY*DCOS(THETA)*DSIN(PHI)+PIX*DCOS(THETA)*DCOS(PHI
124.000      1-PIZ*DSIN(THETA))
125.000       EPHI=(K**2)*(PIY*DCOS(PHI)-PIX*DSIN(PHI))
126.000       MODETH=CDABS(ETHETA)
127.000       MODEPH=CDABS(EPHI)
128.000       POYVEC=((MODETH**2)+(MODEPH**2))/(1.2D2*PI)
129.000       THETA=THETA*57.2957793D0
130.000       PHI=PHI*57.2957793D0
131.000       WRITE(108,23) THETA,MODETH,MODEPH,POYVEC
132.000   23  FORMAT(7X,I3,4X,D16.8,2X,D16.8,2X,D16.8)
133.000       THETA=THETA+10.D0
134.000   100 CONTINUE
135.000       STOP
136.000       END
```

REFERENCES

1. M.V. SCHNEIDER - Microstrip lines for microwave integrated circuits - Bell System Technical Journal, May-June, 1969.

2. W.J.R. HOEFER - Analytical approach to the design of selected microwave integrated circuit structures - Technical Report TR-76-6, April 1976.

3. J. HELSZAJN, D.S. JAMES - Design of microstrip circulators using triangular resonators - Technical memorandum, 31 October 1975.

4. L. LEWIN - "Radiation from discontinuities in microstrip", IEEE Monograph, 358-E, pp. 163-170, February 1960.

5. E.J. DENLINGER - "Radiation from microstrip resonators", IEEE Trans. on MTT, pp. 235-236, April 1969.

6. J. WATKINS - "Circular resonant structures in microstrip" Electronics Letters, 16 October 1969, Vol 5, no. 21 pp. 524-525.

7. P. TROUGHTON - "High Q factor resonators in microstrip" Electronics Letters, Vol 4, pp. 520-522.

8. J. WATKINS - "Radiation loss from open-circuited dielectric resonators", IEEE Trans. on MTT, October 1973, pp. 636-639.

9. B. ESTER, R.J. ROBERTS - "Radiation from half-wavelength open-circuit microstrip resonators." Electronics Letters, Vol. 6, No. 18, 3 September 1970, pp. 573-574.

10. B. EASTER, R.J. ROBERTS - "Microstrip resonators having reduced radiation loss", Electronics Letters, Vol 7, No. 8, 22 April 1971, pp. 191-192.

11. H. SOBOL - "Radiation Conductance of open-circuit microstrip" IEEE Trans. on MTT, November 1971, pp. 885-887.

12. E. BELOHOUBEK, E. DENLINGER - "Loss considerations for microstrip resonators" IEEE Trans. on MTT, June 1975, pp. 522-526

13. J.Q. HOWELL - "Microstrip Antennas", IEEE Trans on AP, January 1975, pp. 90-93.

14. A.G. DERNERYD - "Linearly polarized microstrip Antennas" IEEE Trans. on AP, November 1975, pp. 846-851.

15. P.B. MOREL, S.A. LONG, L.C. SHEN, - "A theoretical investigation of the circular Disc Antenna", Elec. Eng. for this decade (IEEE Region 5) Conf. Digest, University of Texas, April 1976, pp. 286-289.

16. M.D. WALTON, M.R. ALLERDING, L.C. SHEN, S.A. LONG, - "An experimental investigation of the circular disc, printed circuit Antenna", Elec. Eng. for this decade (IEEE Region 5) Conf. Digest, University of Texas, April 1976, pp. 280-293.

17. J.L. ALTMAN - "Microwave circuits", 1964 Van Nostrand, Princeton N.J.

18. A.F. HARVEY - "Microwave Engineering", 1963 Academic Press, London and New York.

19. S. RAMO, J.R. WHINNERY, T. VAN DUZER - "Fields and Waves in Communication Electronics", 1967 John Wiley & Sons, Inc., New York-London -Sydney.

20. S.A. SCHELKUNOFF - "Electro Magnetic Waves", 1945, D. Van Nostrand Company Inc., New York.

21. L. LEWIN - "Advanced theory of waveguides", 1951, Iliffe & Sons, Ltd. London.